UNIVERSITÀ DEGLI STUDI DI PADOVA

DIPARTIMENTO DI BIOLOGIA

Corso di Laurea magistrale in Molecular Biology

TESI DI LAUREA

Generation and characterization of genetically encoded fluorescent probes to visualize mitochondria-endoplasmic reticulum contact sites

Relatore: Prof. Luca Scorrano
Dipartimento di Biologia, Università degli Studi di Padova

Correlatore: Dott.ssa Satoko Shinjo
Dipartimento di Biologia, Università degli Studi di Padova

Laureanda: Aurelia Miscia

ANNO ACCADEMICO 2022/2023

Contents

ABSTRACT

Endoplasmic reticulum (ER) physically contacts mitochondria via its specialized subdomain called mitochondria-associated membranes (MAMs) at sites of mitochondria-ER contacts (MERCs). Interaction between these organelles at the MERCs plays essential roles in lipid and calcium transfer and ultimately in the homeostasis of the two individual organelles. Since the width of the MERCs could be as narrow as 10 nm, which is below the diffraction limit, a handful of probes have been developed to evaluate MERCs formation and dynamics. However, the current probes are dim, or artificially induce tethering, or require complicated imaging procedures that are not compatible with the common imaging setups available to most of the labs. To circumvent these problems, we are developing “STACCATO”, a new generation of probes to visualize MERCs that are based on split Fluorescence-Activating and absorption-Shifting Tag (FAST). STACCATO capitalizes on the reversible nature of split FAST complementation so the probe itself does not work as an artificial tether. In this Thesis we report the generation of a STACCATO probe for MERCs and its initial characterization and we show that STACCATO can report areas of proximity between mitochondria and the endoplasmic reticulum.

CHAPTER 1: Membrane contact sites

Eukaryotic cells maintain homeostasis through the synergetic interaction of organelles with distinct biochemical features. In the last three decades the discovery of contact sites existence between organelles has garnered scientific interest. The contact site can be homotypic (between organelles of the same type) or heterotypic (between organelles of different types) and takes the name of "membrane contact site" (MCS). The relevance of these sites is due to their physiological roles in the cell (Scorrano et al., 2019).

1.1 The birth of the "Membrane contact sites" field

The first observation of intracellular membrane contacts was in the 1950s through electron microscopy (Bernhard & Rouiller, 1956). At that time, free diffusion of soluble proteins and metabolites was considered as the only mechanisms for the communication between intracellular compartments, whereas the active transport of the molecules via the vesicular trafficking was known to be regulated by cytoskeletal elements.(Dennis & Kennedy, 1972). However, after the discovery of mitochondria-associated membranes (MAMs) as a site for phosphatidylserine (PS) synthesis and transport (Vance, 1990) and the other successive achievements referred in the following chapters, the "membrane contact sites" (MCSs) became established as the site of the molecular exchange for intracellular communication. Thanks to the state-of-the-art techniques, such as super-resolution microscopy and focused ion beam-scanning electron microscopy (FIB-SEM), MCSs field has been developed in the last decade. In this context, in 2019, a consensus paper on the classification, characterization and definition of physiological and biochemical role of these structures (Scorrano et al., 2019) has been published, serving as a guideline for the field.

1.2 Features of Membrane contact sites

Membrane contact sites (MCSs) are defined as areas of close proximity between two organelles aimed to facilitate communication. The MCSs are heterogenous being homotypic (between identical organelles), or heterotypic (between different organelles or different membrane types), with different functions. Homotypic interactions, without its fusion, can occur for peroxisomes (Schrader et al., 2000)lipid droplets (Eisenberg-Bord et al., 2016) and possibly for other multicopy organelles.

One of the well-studied heterotypic MCSs is that between mitochondria and endoplasmic reticulum (ER). The mitochondria-ER contact sites (MERCs) play crucial roles on Ca^{2+} regulation and phospholipid synthesis, and consequently on cell death, autophagy, and metabolism (details in Chapter 2). The ER-plasma membrane (PM) contact sites, the other prominent example of heterotypic MCSs, also control Ca^{2+} and lipid homeostasis, with specific regulators (Gallo et al., 2016).

Not limited to these examples, mitochondria form MCSs with endosomes, lysosomes, PM, peroxisomes, vacuoles and nuclear membranes, as well as ER have contact sites with Golgi, peroxisomes and lipid droplets (LDs) (Eisenberg-Bord et al., 2016).

1.3 MCSs tethering proteins

The architecture, the width, and the number of MCSs depend mostly on the recruitment of structural proteins. Tethering proteins often have transmembrane domains or are post-translationally modified with lipidic prosthetic groups, such as palmitoylation (Lynes et al., 2012)that enable them to anchor two organelles. The tethers have functionally distinct domains for other functions than tethering. Extended synaptotagmin1 (E-syt1), for example, is involved in PM-ER tethering, but regulate cytosolic Ca^{2+} levels (Giordano et al., 2013).
The range of MCSs distance is considered between 10 to 80 nm, and each function of MCSs requires a specific range of distances. For example, Ca^{2+} can be transferred from the ER to mitochondria matrix, if they form contact sites closer than 30 nm, according to the molecular structure of channeling complex and their affinity to Ca^{2+} (Giacomello & Pellegrini, 2016).Further introduction regarding to the distance of MERCs will be on the next chapter.

1.4 Ion channeling at MCSs

As mentioned in the previous paragraphs, MCSs play important roles for Ca^{2+} channeling. Intracellular Ca^{2+} levels need to be tightly regulated, mainly but not only, with uptake from outside of the cells through plasma membrane and its storage in the ER. Ca^{2+} concentration in the ER is regulated through the ER-PM MCSs: when Ca^{2+} concentration drops, STIM1 on the ER membrane oligomerize with Orai1 on the PM allowing Ca^{2+} pumping inside the ER (Zhang et al., 2006). Other molecules like small ions, iron etc. may be sorted by the MCSs and nowadays the field is investigating to further characterize these dynamics (Kerner & Hoppel, 2000).

1.5 Lipid channeling at MCSs

Lipids channeling is also extensively documented, dependent on the extent of lipid production/consumption or enrichment of lipid transfer protein (LTP). Ceramides, for example, are produced in the ER and transported to trans-Golgi through CERT. This transport mainly depends on the rate of conversion of ceramides to sphingomyelin and diacylglycerol in the trans-Golgi (Kumagai & Hanada, 2019).
ER-PM MCSs play an important role in maintenance of $PI(4,5)P_2$ levels at the PM. $PI(4,5)P_2$ on the PM should be tightly regulated, because it is a precursor of second messengers such as IP_3, and also contributes for endo- and exocytosis (Balla, 2013).$PI(4,5)P_2$ on the PM can be generated by the phosphorylation of PI4P on the PM. Upon the enrichment of $PI(4,5)P_2$ at the PM, oxysterol binding related proteins 8 (ORP8) is upregulated and transport PI4P from PM to ER and

PS from ER to PM, as a counteract, at PM-ER contact sites, to suppress further PI(4,5)P_2 production (Sohn et al., 2018).On the other hand, phosphatidic acid (PA) enrichment on the PM facilitates Nir2/3 activity for the transfer of phosphatidylinositol from ER to PM, to replenish the source of PI(4,5)P_2 (Chang & Liou, 2015).
MCSs are frequently enriched with lipid transport proteins (LTPs) which drives for lipid channeling. The unique lipid composition of the membranes at MCSs recruits resident LTPs and, on the other hand, LTPs regulate composition of the membranes. LTPs also mediate lipid transfer when vesicular transport is impaired (Prinz et al., 2020). LTPs maintain gradient of sterol concentration in two organelles by regulating their transport. For instance, Osh4p is an LTP involved in lipid transfer from ER to Golgi against gradient and counter exchanging PI(4)P from the Golgi to the ER (von Filseck et al., 2015).As another example: vesicle-associated membrane proteins (VAMP)- associated proteins (VAPs) regulates the sterol transport from ER to PM(Quon et al., 2018).

1.6 ROS signaling

Reactive oxygen species (ROS) represent one of the mechanisms of cell signaling at MCSs. Ca^{2+} transport from ER to mitochondria facilitates influx of K^+ and water into the mitochondrial matrix. This flux then stimulates H_2O_2 translocation from the mitochondrial cristae to MERCs. The ROS release results in positive feedback of Ca^{2+} oscillation and affects IP_3R activity (Booth et al., 2016).

1.7 Enzymes signaling

Cell signaling can also depend on phosphorylation state of receptors. Tyrosine kinase receptors on the PM are dephosphorylated at the MCS with the ER by protein-tyrosine phosphatase 1B. Phosphatase 1B is an ER enzyme “working in trans” so that its substrate is on the PM. This is an example of a common mechanism of signaling regulation in MCSs (Haj et al., 2012).

CHAPTER 2: MERCs and MAMs

2.1 MAMs and MERCs definition

The Mitochondria-associated ER-membranes (MAMs) fraction was first identified in 1990 by J. E. Vance. In this study, she found that phosphatidylserine synthesis occurs mainly in the so-called “fraction X”, which is associated with the “crude mitochondria” fraction but displays a lower sedimentation rate than “pure” mitochondria in further separation by ultracentrifigation on a Percoll gradient. This fraction, nowadays called MAMs, was subsequently established as the main site of production of some lipids such as phosphatidylethanolamine (Vance, 1990).

MERCs are a platform where Ca^{2+} and ion exchange between the two organelles, lipid synthesis, mitochondrial fusion and fission, inflammasome initiation and autophagosome formation happen. The field of MAMs is increasingly attracting the interest of scientists, considering the recent findings regarding Alzheimer's disease, amyotrophic lateral sclerosis, and type 2 diabetes mellitus, as in obesity, GM1-gangliosidosis, and viral infection by human cytomegalovirus or hepatitis C (Janikiewicz et al., 2018).

In this context, MERCs (mitochondria-ER contact sites) is used as a technical term to describe structural architecture of the contact sites between mitochondria and ER. On the other hand, the term MAMs refers to the biochemical nature of MERCs including the pool of proteins and lipids that define mitochondria-ER contact sites. In past years, more than 1000 proteins have been defined as “MAMs localized proteins”, but further studies are necessary to characterize the MAMs resident proteins (Giacomello & Pellegrini, 2016; Yang et al., 2020).

2.2 MERCs thickness

Mitochondria form contacts with the smooth endoplasmic reticulum (MERCs) and with the rough endoplasmic reticulum (ribo-MERCs).

MERCs thickness ranges from 10 to 25 nm, meanwhile ribo-MERCs distance ranges from 50 to 80 nm. The minimal size of the ribo-MERCs observed is 20 nm to accommodate ribosomes. These distances vary according to the metabolic state of the cell (Anastasia et al., 2021).The number of MERCs instead increases in cellular stress conditions (Csordás et al., 2006; Giacomello & Pellegrini, 2016).

2.3 MERCs as site of lipid biosynthesis and trafficking

Phosphatidylserine, triacylglycerol and steroids are all produced at the MERCs. Stone J.S. and Vance J. showed in 2000 that MAMs are heavily enriched in phosphatidyl synthase 1 and 2 (PSS)1/2 and the major site of phosphatidylserine synthesis. Phosphatidylcholine is a major component of cell membranes, generated by the phosphatidylserine decarboxylation in the mitochondria and successive processing by phosphatidylethanolamine N-methyltransferase-2 in the ER (Stone & Vance, 2000; van der Veen et al., 2017).

The thickness of the MERC does not affect the lipogenesis because this depends on the number of lipid-MERCs. The lipid channeling instead depends on the distance between the organelles. It is supposed, in fact, that lipids are transported through hydrophobic channels that would be disrupted if the thickness of the MERC increases. Another proposed mechanism is based on the diffusion of lipids coated by proteins and diffusion dynamics follows Fick's and Einstein's (Schauder et al., 2014).

2.3 Ion exchange

2.3.1 Ca^{2+} flux at the MERCs

Ca^{2+} is one of the most important molecules used for signaling in the cell such as induction of apoptosis, regulation of cellular metabolism, neurotransmitter release, and cell proliferation ((Clapham, 2007). Thus, the level of free Ca^{2+} in cytosol must be fine-tuned. Free intracellular Ca^{2+} is delivered by Ca^{2+} ATPases: Plasma membrane Ca^{2+} ATPase PMCA on the plasma membrane and sarco/endoplasmic reticulum (SERCA) on the ER. The ER is the main storage site for Ca^{2+} in the cell, heavily equipped with Ca^{2+} transporters as inositol-1,4,5-trisphosphate receptor (IP3R), ryanodine receptor (RyR), SERCA and Ca^{2+} binding proteins as calreticulin, calsequestrin, and immunoglobulin binding protein (BiP) (Berridge, 2016).
IP_3R is responsible for Ca^{2+} release from ER to mitochondria, stimulated by IP_3, and regulated by sigma1R, Bcl-2 etc (Filadi & Pozzan, 2015). Ca^{2+} flow from ER to mitochondria is affected by the width of the MERC cleft: increasing the distance between the two organelles the diffusion slows down in a proportional way. The distance is crucial to allow the optimal Ca^{2+} flux, because IP3R on the ER and VDAC on the OMM are required to be tethered with Grp75. The optimal width for Ca^{2+} transfer is at 15nm: The MERCs distance greater than 24 nm does not allow the assembly of the complex, meanwhile a distance less than 12 nm would cause steric hindrance of the channeling proteins impeding Ca^{2+} flux (Giacomello & Pellegrini, 2016).
FRET can be used to detect conformational changes of a macromolecule upon binding of a ligand by fusing one terminus of the molecule in question with the donor fluorophore and the other end with the acceptor fluorophore. To evaluate Ca^{2+} fluctuations in MERCs, tandem GFP probes designed with a calmodulin domain linking the two donor and acceptor ends of the fluorophore were used: Ca^{2+} oscillations could enhance or repress FRET signal (Miyawaki et al., 1997).
IP_3R1 subunit interacts with BH4 domain of Bcl-2; this association is sufficient to block Ca^{2+} flux and apoptosis. Bcl-2 inhibitor HA14-1 causes mitochondrial Ca^{2+} oscillations via IP_3R1, leading to the mitochondrial membrane permeabilization, cytochrome C release, and eventual apoptosis (Monaco et al., 2012).
ER stress associated ROS production facilitated Ca^{2+} flux through PERK mediated MERCs tethering, causing apoptosis (Verfaillie et al., 2012).
2.4.2 Ion trafficking at MERCs

MERCs dynamics may be involved in the passage of ions other than Ca^{2+}; in particular, Zn^{2+}, which regulates tricarboxylic acid cycle and electron transport chain (X. Liu et al., 2019)Zn^{2+} can inactivate mitochondrial biogenesis and DNA replication in mitochondria of hepatocytes, while it is abundantly present in cortical neurons to manage the huge demand of ATP.
Cu^{+} is fundamental in mitochondria where it assembles in redox centers by cytochrome C oxidase and SCO1, SCO2 chaperons. It is hypothesized that Cu^{+} flows through a transporter at the MERCs able to transfer Cu+ from the ER to the other cellular compartments (H. Y. Liu et al., 2021).

2.4 MERCs tethers/regulators

Nowadays it is known that IP_3R on the ER and voltage-dependent anion channel 1 (VDAC1) and on the outer mitochondrial membrane (OMM) act as tethering complex together with Grp75 (Szabadkai et al., 2006). MFN1/2 (de Brito & Scorrano, 2008). And ERMIT2, the new MFN2 variant (Naón et al., 2023). PACS-2 (Simmen et al., 2005), PTPIP51-VAPB (De Vos et al., 2012).

2.5 MERCs regulates mitochondrial fusion and fission.

Mitochondria undergo fusion and fission events corresponding the physiological and metabolic state of the cell. It has been observed that fission events happen more frequently in pathological states of the cell and in particular in neurodegenerative diseases than in cells at physiological state. MERCs mark the division site according to the fact that the ER constrict the mitochondrion in the points where Drp1 would be recruited and the division happens (Friedman et al., 2011).
Mitochondria fuse thanks to three GTPases, Mitofusin1 (MFN1), Mitofusin 2 (MFN2), for OMM fusion, and Optic atrophy protein 1 (OPA1) for IMM fusion. Abrisch et al. reported that the mitochondrial fusion sites colocalize with MERCs, so that MERCs might be the crucial sites to regulate mitochondria morphology in both process: fusion and fission (Abrisch et al., 2020).

2.6 MERCs and autophagy

Autophagy is a fundamental process for the cell to recycle material or degrade harmful cellular elements to ensure homeostasis. This process begins with the elongation isolation membranes, that forms autophagosome later engulfing the materials. The origin of the isolation membrane has been debated for a long time but Hamasaki et al. demonstrated that this membrane derives from MERCs (Hamasaki et al., 2013).In particular, it has been observed at TEM that ATG14, a marker for autophagy initiation, localizes at the MERCs during starvation at a distance of 50 nm or more.

2.7 MERCs in health and disease

Recent studies revealed that MERCs play roles in disease progression. For example, MERCs in neurons are involved in production of amyloid β from the β secretase- mediated cleavage of palmitoylated amyloid precursor protein (APP). Aβ accumulation ends in plaques of agglomerated proteins which are neurotoxic and that are the major cause of Alzheimer. According to these findings MERCs have a fundamental role in regulation of lipid homeostasis and can be a target for treatment of neuro degenerative diseases (Bhattacharyya et al., 2021).

2.7.1 MAMs role in senescence and aging

Cellular senescence is a physiological process to which the cell undergoes and that ends with proliferation arrest and pro-inflammatory secretome formation. According to the fact that senescence is stress driven, Ca^{2+} flux in MAMs is upregulated in senescence to be then accumulated in mitochondrial matrix . In this context the protein ITPR2, together with the proteins canonically known to be involved in ER-mito Ca^{2+} transfer, favors senescence induction. Moreover, increase in number of MERCs is also denoted in senescent cells (Ziegler et al., 2021).

Aging is a physiological process during which oxidative stress, ROS and DNA modifications accumulation, inefficient organelle turnover and impaired proteostasis happens at cellular level. While senescence can be defined as “an irreversible form of long-term cell-cycle arrest, caused by excessive intracellular or extracellular stress or damage”, aging is “the time-relating irreversible proliferative deterioration of those physiological processes of the organism that support its survival and fertility” (Dodig et al., 2019).

MAMs play a role in ROS regulation in aging cells according to the fact that Ca^{2+} transfer in MAMs affects Krebs cycle, ATP synthesis, mitochondrial transition pore (PTP) opening and more importantly mitochondrial respiratory chain and membrane potential. These two last effects, together with aging associated with RyR destabilization, cause an increase in ROS production. MAMs proteins that participate in ROS production are Ero1-Lα and PDI that catalyze disulfide bonds formation in newly synthetized proteins discharging electrons in H_2O_2 and P66hc MAM-localized cause indirect cytochrome c oxidation by formation of H_2O_2 radical species participating, in this way, in apoptosis induction (Janikiewicz et al., 2018).

2.7.2 MAMs role in breast cancer

MAMs are critical in the establishment of breast cancer. MAMs architecture and proteome, indeed, are deeply altered during this malignancy. In breast cancer several mechanisms stress-induced are verified: in early onset, chaperone sigma-1 receptor (Sig1R) expression is increased and this protein detaches from BiP/GRP78 chaperone complex to which binds in physiological conditions to associate with IP3R increase ER-mito Ca^{2+} fluxes. In prolonged ER stress, Sig1R can stably move from MAM to the periphery of the ER. These mechanisms are all

aimed to limit cell damage are regulate cell death, while, to promote cell invasiveness in breast cancer, Sig1R associates with SK3 potassium channel and Orai1 (Yu et al., 2021).
In cancer, in particular in breast cancer, it can be observed the increase in number of IP3R. KO of this receptor ends in increase in LC3-II and in ROS production leading to autophagy, tumor growth suppression and cell death. This, together with the previous findings suggest that arrest of Ca^{2+} flux in MAMs which depends on alteration in co-functioning of IP3R with Akt/mTOR, cause disruption of MAMs architecture and bioenergetic imbalances in mitochondria that end to kill the affected cancer cells (Morciano et al., 2018).

2.9 MAMs role in inflammation

Inflammation initiation requires the assembly of inflammasomes, multiprotein complexes able to sense pro-inflammatory antigens, activate cysteine protease caspase-1 and so regulate maturation of proinflammatory cytokines (IL-1, IL-18). There are four subfamilies of inflammasomes but the most frequently involved in human pathogenesis is the NOD-like receptor protein 3 (NLRP3). NLRP3 are localized on the ER in inactive state but after their activation, whose mechanisms of initiation are still under study, NLRP3 move to MAMs together with its adaptor ASC where they perceive ROS accumulation and DAMPs coming from mitochondrial of cells in a pathological condition (Missiroli et al., 2018).

2.10 MAMs in infections

Other than the well-established mechanism of MAMs involvement in inflammasome formation it is worth to note that MAMs participate also in immune viral response. Mitochondrial antiviral-signaling protein (MAVS) and retinoic acid-inducible gene-I protein (RIG-I) are proteins localized at outer mitochondrial membrane, peroxisomes and MAMs that induce the release of pro-inflammatory cytokines from the virally infected cell upon its activation. Stimulator of interferon genes (STING) plays crucial roles in stimulating the pro-inflammatory response to viral infection. According to this it has been observed that, upon infection, STING binds to MAVS and RIG-I in MAMs; mechanism through which the anti-viral, pro-inflammatory response in potentiated and incorporated at the level of MAMs and it directs viral tactics to reduce or stop the triggering of the interferon (IFN) response and to disrupt the proper functioning of MAMs (Missiroli et al., 2018)
During infections of human cytomegalovirus, moreover, it has been seen a notable systematic increase in MERCs number in particular in infected fibroblasts. MAMs in cytomegalovirus infected cells are altered with an increase in HSP60 and BiP chaperones fundamental for the assembly of the virus. In these conditions also glucose regulated protein 75 (Gpr75) and voltage dependent anion channel (VDAC), the main proteins involved in Ca^{2+} transfer between ER and mitochondria, are increased together with the increase of proapoptotic regulatory proteins concentration in MAMs. So MAMs definitely have a multiple and varied

role in regulation of inflammation signaling and infections dependent cellular responses (Zhang et al., 2006).

CHAPTER 3: Techniques to study MAMs

3.1 Fractionation

Fractionation has been used to define the biochemical composition of MAMs. Through this technique, membrane contact sites are obtained by ultracentrifugation. SDS-PAGE can then be performed on the isolated fractions to define the resident proteins. Heterotypic contacts can display protein composition either of one organelle or of both organelles involved in the MCS either unique of the contact region. The fractionation method requires optimization of the protocol to obtain pure fractions. Moreover, fractionation is not suitable to identify transiently localized proteins.

3.2 Microscopy

3.2.1 Electron microscopy

MERCs were first observed in 1950s through transmission electron microscopy (TEM)(Bernhard & Rouiller, 1956). TEM is a microscopy technique used to observe ultrastructure in cells with ~0.1 nm of resolution. Because of its high resolution, TEM is the gold standard to visualize architecture of the MERCs. Furthermore, the combinations with confocal microscopy (Correlative light and electron microscopy, CLEM) and immunogold staining enable us to investigate the precise localization of MERCs resident proteins. This technique can be used only with fixed samples; therefore, it is not suitable to examine dynamic changes of MERCs (Scorrano et al., 2019).

3.2.2 Electron tomography (ET), cryo-electron tomography cryo-ET and FIB-SEM.

Electron tomography, cryo-electron tomography and scanning electron microscopy present some advantages with respect to the traditional TEM. 3D tomography from TEM images of serial sectioning is the common method to understand organelle ultrastructure including mitochondrial cristae, and also mitochondria-ER contact sites (de Brito & Scorrano, 2008). Each section has from 1 to 10 nm width, which corresponds to z-axis resolution. For the classification of the organelles, manual selection has been required, however, several groups developed tools for organellar segmentation automatically with machine learning. In cryo-ET the sample is vitrified in liquid ethane; this technique has the ulterior advantage respect to standard ET to give more resolution and completeness to the final 3D reconstruction: cryo-ET limits the regions empty of information the "missing wedges" (Wolfgang et al. 2022).
Focused ion beam scanning electron microscopy (FIB-SEM) uses gallium electron beam to cut the sample therefore the z-axis resolution reaches to 3 nm, which is thinner than 3D tomography (Peddie et al. 2014) This state-of-art technique visualizes all the organelles structure in 3D. Like 3D tomography,

organelle segmentation requires manual selection of the boundary of each organelle, however, automatic tools are available nowadays.

3.2.3 Fluorescence Microscopy

Proteins functionally and structurally involved in MCSs can be fused with fluorophores in order to be visualized at confocal fluorescent microscope or at super resolution microscopes. Application of STED, STORM and PALM microscopy techniques for the visualization of these fluorescent tags can be used to determine the precise localization of the protein of interest (Owen et al. 2012).

3.2.3.1 Förster resonance energy transfer (FRET)

Förster resonance energy transfer (FRET) is a fluorescent microscopy technique appliable in living cells used to determine the proximity between two proteins. In FRET, the energy from donor fluorophore transmits to excite the acceptor fluorophore, if the proximity requirements are met. By calibration of the emitted fluorescence signal, it is possible to assume the proximity between the two proteins in a range between 1 and 10 nm. These features make FRET a suitable technique to estimate the distance between two subcellular compartments of the cell in close proximity, for example to define the distance between two organelles in MCSs (Csordás et al., 2010, Molecular Cell, doi: 10.1016/j.molcel.2010.06.029).
The most common and significant problem of FRET is to have the need to have the two fluorophores in the same stoichiometric ratio: if one fluorophore is in excess respect to the other, significant background would be detected in the acquisition. (Piston et al.).
FRET indices respond nonlinearly to changes in degree of molecular interaction (the distance between the two probes is computed as

$$R_0 = 0.02108\,[k^2 \times \Phi_D \times n^{-4} \times J]^{1/6}$$

(Shrestha et al., 2015) and are not standardized among different optical imaging devices and different laboratories making harsh the correct interpretation of the results (Zal & Gascoigne, 2004).
Another limitation of FRET is the low signal to noise ratio that affects the resolution of this imaging technique. Protein-protein interactions studies or MCSs dynamics observations require a large number of measurements which can end in bleaching of the fluorophore and reduction of the signal that is naturally low compared to the background. In order to perform the necessary number of measurements before the fluorophore bleaches, it is fundamental to optimize the quantum yield of the system (Woehler et al., 2010).
FRET can be combined with other techniques such as fluorescence lifetime imaging (FLIM) to study the MCSs proximity with high temporal resolution (Venditti et al., 2019). Photoswitching FRET and photobleaching FRET are also other techniques that are alternatives to the original FRET in which the acceptor is bleached instead of excited (Huang et al., 2019).

FRET photobleaching works in detecting FRET efficiency, so to determine how much donor fluorescence is lost because of the energy transfer, by measuring timing and intensity of donor emission recovery after acceptor photobleaching. Photoswitching FRET overcomes some limits of FRET photobleaching as the impossibility to make several FRET analysis on the same sample due to the irreversible photobleaching of the acceptor fluorophore, or complications due to incomplete photobleaching, or eventual photoconversion of the acceptor fluorophore in a fluorescence state belonging to the donor spectrum. Photoswiching FRET uses photoswitchable acceptors that instead of being bleached can be simply turned on or off after receiving a suitable laser pulse (Bastiaens et al., 1996; Rainey & Patterson, 2019)

3.2.3.2 Bioluminescence resonance energy transfer (BRET)

Bioluminescence resonance energy transfer (BRET) is another technique to study protein-protein proximity. The energy from oxyluciferin catalyzed by luciferase is transferred to fluorescent protein to emit fluorescence, only if they are closer than 10 nm. Hertlein et al. developed MERLIN (Mitochondria–ER Length Indicator Nanosensor) applying BRET to MERCs. They targeted renilla luciferase on the ER membrane and Venus, yellow fluorescent protein, on the outer mitochondria membrane, and demonstrated that the BRET is dependent on the expression level of MERCs tethers such as MFN2 and PDZD8 (Hertlein et al., 2020).

3.2.3.3 Dimerization-dependent fluorescent protein (ddFP)

Dimerization-dependent fluorescent proteins are genetically encoded proteins monomer which emits fluorescence only upon binding to another monomeric ddFP. The first ddFP system developed was ddRFP derived from dTomato. This system was then optimized in order to solve the limits of low brightness, low signal to noise ratio and limited color palette. Through direct evolutional mutagenesis, Campbell's group generated ddGFP and ddYFP which display a stronger fluorescent signal than ddRFP(Alford, Abdelfattah, et al., 2012). These fluorophores can be used to study protein-protein interaction. This technique was applied to visualize MERCs (Alford et al., 2012).ddGFP monomers, ddGFP-A and -B, were targeted to the outer mitochondrial membrane and to the endoplasmic reticulum membrane, respectively. When the distance between these two organelles approaches <20nm the emitted signal is enhanced. ddFP system has the advantage to be fully reversible because the monomers dimerize with interactions of high dissociation constant, a feature that makes this technique suitable to study MERCs dynamic changes without artifact generation.
Recently Miner et al. developed Contact-FP: a split fluorescent reporter developed from ddFP that, according to the type of target to which it is fused, is able to detect various MCSs. Through the use of Contact-FP it was possible to visualize MCSs mainly between lipid droplets and mitochondria but this probe can potentially be used to detect other types of MCSs. Contact-FP has the advantage

of implication of reversible interactions but the disadvantage of low signal to noise ratio (Miner et al. 2023).

3.2.3.4 Bimolecular fluorescence complementation (BiFC)

BiFC is a fluorescence tool for visualization of protein interaction and subcellular localization assessment of tagged protein complexes in cells. In BiFC, a fluorophore is split in two non-fluorescent fragments, and these two fragments can be complemented as a fluorescent protein, upon interaction (Huang et al., 2019; Kerppola, 2008).

BiFC enables us to visualize the interaction of interest in living cells. An advantage is that BiFC signal is specific from the complementation allowing the visualization of the exact proteins of interest (Lai & Chiang, 2013).

SPLICS is a fluorescent sensor from MERCs detection developed from splitGFP principle, fusing splitGFP C-terminus and N-terminus with mitochondria and ER targeting sequences. It was designed in two variants to detect MERCs of two widths (Cieri et al., 2018).

The complemented fluorophore from splitGFP system has slow maturation time ($T_{1/2}$ ~ 1 h) which is inappropriate to study transient/dynamic interactions. Furthermore, reconstitution of splitGFP has much less dissociation constant (78,8 pM) than other systems such as ddGFP (Kd = 9μm) and several transient protein interaction (fos-jun Kd = <1nM, ERK-MEK Kd =50nm), which means complemented GFP can be considered as irreversible. Therefore, suitable negative controls for protein interaction such as mutation on the binding site are required.

3.3 Proximity labeling

3.3.1 BioID

BioID is a technique used to detect all transient and stable interactions between the protein of interest and the surrounding molecules. It employs a mutated version of BirA (an enzyme of bacterial origin able to inactivate biotin synthesis operon and biotinylate acetyl-CoA carboxylase with biotin bound to AMP) with lower affinity for BioAMP. Proteins of interest are engineered with mutated BirA so that all proximal interactors would be biotinylated, isolated through a pull down assay and identified through mass spectrometry. BioID split can be used to label 2 opposite membranes in a contact site and biotinylate molecules in the cleft. BioID was employed to define proteins tethering mito-ER, for the definition of PEX16 interactome in the ER in the process of peroxisomal biogenesis, for the characterization of the role of PERK in MERCs (Huang et al., 2019)

3.3.2 APEX

This technique can be used as an alternative to BioID. APEX uses a mutated version of ascorbate peroxidase which in presence of hydrogen peroxides and biotin-phenol is able to form biotin-phenoxyl radicals which attach to proximal proteins labeling them. A split version of APEX can be used for complementation assay in membrane contact sites tagging the proteins localized in the region of

interest. Thanks to APEX it has been discovered that ATL2 with RTN1 and RTN3, in HEK293, and SYNJ2BP with RRBP1 are tethers of MERCs (Huang et al., 2019; Scorrano et al., 2019).

3.3.3 Proximity ligation assay

This method allows us to visualize protein-protein interaction in the region of interest. The two proteins in question are bound to each primary antibody, then bound to species-specific secondary antibodies linked to two different oligonucleotides. If the two proteins are 20-40 nm, upon addition of the connector oligonucleotides and enzymes, rolling circle amplification happens, and fluorescent oligonucleotides give signal. This system is commonly used to quantify MERCs by tagging IP3R and VDAC1 (Huang et al., 2019; Young, 2019).

3.3.4 Pull down

With this assay it is possible to catch interacting proteins in cell lysates, purified proteins, expression systems and in vitro transcription/translation systems. The protein of interest is tagged with a bait and immobilized on a support by affinity tag. The other proteins (preys), coming from the cell lysate or one of the other systems mentioned above, are caught by the bait. The final complexes are then eluted, purified and analyzed at mass spectrometry. This method has been used to confirm that (VLGR1), a protein associated with human Usher syndrome, interacts with MAMs main resident proteins and that VLGR1 KO causes disruption of MAMs architecture (Louche et al., 2017).

CHAPTER 4: Fluorescence- activating and light absorption shifting tag (FAST)

FAST (Fluorescence-activating and light absorption shifting tag) is "a novel protein tag able to fluorescently label livings cells and multicellular organisms" developed in Prof. Gautier's group. This probe is normally non fluorescent, switching instantaneously to an high fluorescent signal when it reversibly binds to a cell permeant fluorogen that works as a cofactor. The full reversibility of the fluorogen binding to the active site of the probe allows us to study the same cells in sequential different conditions: cells can be treated again with the fluorogen after it has been washed out. This feature also allows FAST to overcome the problem of photobleaching. The size of FAST is smaller than that of GFP (roughly half), thus avoiding steric hindrance in the site of FAST expression and simplifying the cloning procedures to generate FAST-based probes and tags (Plamont et al., 2016).

4.1 FAST design

FAST has been engineered by direct evolution of photoactive yellow protein (PYP). PYP is a monomeric protein of 14-kDA so half of the size of GFP.
PYP is a model photoreceptor discovered in *Halorhodospira halophila* that enables the bacterium to sense blue light upon binding of *p*-coumaric acid . There exists many versions of PYP which have Tyr42, Glu46 and Cys69 as conserved residues among the different bacteria phyla. The function of this protein is not completely understood but it seems that PYP activation in *H.halophila* is involved in motility and biofilm formation (Xing et al., 2022).
PYP covalently binds parahydroxycinnamoyl chromophore (HC) in phenolated deprotonated form to its Cys69 residue to sense blue light. FAST uses PYP as scaffold and 4-hydroxybenzylidene-rhodanine (HBR) or 4-hydroxy-3-methylbenzylidene-rhodanine (HMBR) as fluorogens. The first to be chosen as fluorogen was HBR because of its structure, analogous to GFP, and because HBR has a redox center between its phenol and rhodamine groups. The electron donation from phenolate deprotonates HBR and makes this molecule able to undergo a red absorption shift of 50nm; so HBR must be stabilized in its deprotonated form in order to emit fluorescence. According to the fact that PYP stabilizes HC in a deprotonated form and that HBR shares structural similarities with HC, the active site of PYP was mutagenized to hold deprotonated HBR. The mutant most successful displayed HBR fluorescence at ~530nm being excited at ~470nm. HBR:Y-FAST showed 9% quantum yield meanwhile HMBR, an analog of HMBR resulting from the screening showed 33% quantum yield (Plamont et al., 2016).

4.2 SplitFAST

From the design of FAST, SplitFAST probe was generated. SplitFAST allows to monitor in real time the formation and dissociation of protein assembly or to

detect MCSs. SplitFAST can cover all the fields in which BiFC is usually adopted: this novel probe in fact it is based on the same principle of fluorescence emission upon protein complementation of BiFC but having unique advantages respect to the usual split fluorescence reporter. SplitFAST, in fact, is the FAST probe divided into its Ser 114 and Gly 115 with the residues from 1 to 114 being the N-FAST and the residues from 115 to 125 terminus being C-FAST. Alternative versions of SplitFAST can be obtained by the removal of C terminus residues; doing so C-FAST10-8 is produced which has lower affinity for N-FAST respect to the standard C-FAST11 and so has a broader dynamic range. Protein complementation as well as fluorescence emission in splitFAST is reversible because the split protein reconstitute and fluoresce only when the exogenous fluorogen is subministered to the medium in a mechanism identical to FAST. SplitFAST respect to BiFC has reversible and fast chromophore maturation which allows to monitor also transient complexes and intermediate stages without creating hypothetical artifacts that can derive from the irreversible maturation of GFP chromophore. Moreover, the small size of splitFAST avoids the steric hindrance that can be caused by GFP split probes (Tebo & Gautier, 2019)

4.3 SplitFAST for MERCs detection

Although there are different methods for MERCs analysis (described in Chapter 3) electron microscopy (EM) remains the golden standard for MERCs studies. However, because EM requires fixation of the samples, it is not suitable to explore dynamic changes in MERCs. Fluorescent microscopy represents a suitable alternative to EM, and it can be used to visualize sites of contact in live cells, but its resolution is much lower than EM. SPLICS that are BiFC-based probes more precise than standard fluorescent microscopy, display the highest signal to noise ratio, but are irreversible and their reconstitution occurs slowly, thereby introducing artifacts and limiting the possibility to study the dynamic changes in MERCs. FRET- and ddGFP-based probes do not induce artificial tethering, but are complicated to image or display a low signal-to-noise ratio. To overcome these limitations, we need easy to image, reversible MERCs probes capable of measuring them at various widths and displaying a signal-to-noise ratio. A possible probe is based on a bright, genetically encoded split fluorescent protein, targeted only to MERCs where it reconstitutes without inducing artificial tethering. Thus, the proposed probe shall display a dissociation constant K_D (eq. 1)

$$K_D = \frac{[A]^x[B]^y}{[A_x\ B]_y} \qquad \text{(eq. 1)}$$

that is high enough to prevent the induction of artificial bridges between the two organelles, when expressed and reconstituted. We therefore inspected the K_D of the probes currently in use and of well-known protein-protein interactions in

cellular environments (Figure 1). The higher the K_D, the greater the reversibility of the binding. BiFC K_D is 78.7 pM (Do & Boxer, 2011), while the K_D of ddGFP is ~9 µM (Alford, Ding, et al., 2012), suggesting that ddGFP is much more reversible than BiFC system in the cells. Thus, the K_D of the newly designed probe should be in the range of 10s of µM. In addition, such a probe shall display a high signal-to-noise ratio to facilitate its imaging under a variety of conditions.

Interaction type	**Dissociation constant** $\boldsymbol{K_D = \frac{[A]^x[B]^y}{[A_x\ B]_y}}$	**Reference**
ddGFP-A and B	9 µM	(Alford, Ding, et al., 2012)
Split FAST	0.21-25 9 µM	(Tebo & Gautier, 2019)
MEK and ERK	0.1 µM	(Fujioka et al., 2006)
FKBP an FRB + rapamycin	12 ± 0.8 nM	(Banaszynski et al., 2005)
Fos and Jun	0.99 ± 0.30 nM	(Heuer et al., 1996)
SplitGFP	78.7 ± 13.8 pM	(Do & Boxer, 2011)

Table 1. K_D of bimolecular probes currently in use and of interacting protein-protein couples.

As mentioned above, upon irreversible binding of its cell permeant fluorogen, (Lime and Coral) FAST displays a high signal-to-noise ratio, similar to that of GFP (Plamont et al., 2016). In addition, a split version of FAST is available, where its C- and N-terminus fragments can self-complement to reconstitute a full FAST that becomes fluorescent when bound to its fluorogen (Tebo & Gautier, 2019). Thus, in principle, splitFAST can represent a useful tool for the generation of a MERCs probe. Moreover, the K_D between C-FAST10 or C-FAST11 and N-FAST in the presence of the different fluorogen falls in the µM order, comparable to that of the ddGFP system (Table 2) (adapted from Tebo et al., 2019).

C-FAST versions	**sequence**	**K_D (µM) + Coral (10 µM)**	**K_D (µM) + Lime (10 µM)**
C-FAST11	GDSYWVFVKRV	0.21 ± 0.05	1.4 ± 0.2
C-FAST10	GDSYWVFVKR	0.95 ± 0.08	6.2 ± 0.5

Table 2. K_D of C-FAST10 and C-FAST11.

SplitFAST preserves all the features of the FAST probe itself with the same excitation and emission wavelengths, signal-to-noise ratio and speed of fluorogen binding kinetics. SplitFAST reconstitution is very fast, suggesting that this probe is also suitable to detect transient interactions. Thus, SplitFAST appears to be suitable for the visualization of MERCs, upon targeting of each of its halves to mitochondria and to the ER.

CHAPTER 5: Purpose of the thesis

Given the importance of MERCs in cell physiology and pathology and the need for specific, easy to use, reversible, bright and flexible probes to dynamically visualize this interface and quantitatively measure its extent and changes in varying conditions, the Purpose of this Thesis has been to generate and characterize a MERCs probe based on the SplitFAST technology. We describe the characterization and validation of 9 different versions of such a probe. We show that the C- and N-terminus of FAST are properly localized to the surface of the intended organelle and that the two different probes tested in this Thesis can detect the proximity between ER and mitochondria.

CHAPTER 6: Materials and methods

6.1 Cell culture

U2OS were cultured at 37°C in a 5% CO2 atmosphere in high glucose (5.4 g/L) Dulbecco's Modified Eagles Medium (HG-DMEM, Invitrogen, #11965092) supplemented with 10% Fetal Bovine Serum (FBS, Thermo Fisher scientific, #26140079), 1% non-essential amino acids (MEM Non-Essential Amino Acids Solution (100X) Thermo Fisher scientific, #11140050) and 1% Penicillin-Streptomycin (PS, Thermo Fisher scientific, #15140122). U2OS grow 10 times with a coefficient of 1.8 each overnight from the initial seeding number. The first day 16500 cells were seeded in Cell culture flask, T-75, surface: Standard, Filter cap #3023421 SARSTEDT. U2OS cells were kept subconfluent with splitting 1:10 every 5 days. In detail, subconfluent cells were rinsed in 1x PBS, trypsinized (trypsin solution: 0.05% Trypsin, 1x PBS, 0.53 mM EDTA, 0.2 g/l glucose, 0.07 g/l $NaHCO_3$) and subcultured in the complete DMEM. Upon transfection, transfected cells are cultivated in antibiotics-free DMEM; after 48 hours the medium has been changed to the complete one.

6.2 Colony Polymerase Chain Reaction

Colony PCR was performed to screen the bacterial colonies. Each colony was mixed with 10 µl of PCR mix (5 µl KAPA2G Fast ReadyMix Roche #KK5103, 1 µl of 2 µM forward primer*, 1 µl of 2 µM reverse primer*, 3 µl ultrapure water) in PCR tube (SARSTEDT #S044082). The sequences of the primers are shown in Table 3.

	AKAP-L(n)-C-FAST11	AKAP-L(n)-C-FAST10
Fwd primer	CMV-F: 5'-CGCAAATGGGCGGTAGGCGTG -3'	CMV-F: 5'-CGCAAATGGGCGGTAGGCGTG -3'
Rev primer	5'-CCCTGAACCTGAAACATAAAATG -3'	5'-CGCAAATGGGCGGTAGGCGTG -3'

Table 3. Primer sequences for colony PCR

The DNA was amplified in MiniAmp Thermal Cycler by Thermo Fisher Scientific according to the following set up:

Step 1	95 °C	3 minutes	
Step 2	95 °C	15 seconds	x35
	60 °C	15 seconds	
	72 °C	10 seconds	
Step 3	72 °C	30 seconds	

The samples were run in 2% agarose gel in TAE 1x buffer at 90 V.

6.3 Transformation and DNA extraction

XL10-Gold Ultracompetent Cells (Aglilent, #200315) were incubated with 4µl of DNA for 30 minutes. Bacterial membrane was permeabilized with incubation at 42°C for 45 seconds and then transferred immediately on ice. As for the transformation of the plasmids with kanamycin resistant gene cassette, the competent cells were cultivated in 2ml of LB for 30 minutes at 37°C. The cultured bacteria were then centrifuged at 5000 xg for 5 minutes at RT, pellet with 100 µl of supernatant was plated on LB-agar plates supplemented with kanamycin (50 µg/ml) and cultivated for 15 hours at 37°C. For the plasmids with ampicillin resistant gene cassette, the competent cells were directly plated on LB-agar plates supplemented with ampicillin (100 µg/ml) and cultivated at 37°C for 15 hours. Transformed colonies were screened with colony PCR (details are in section 6.2). Mini culture was performed on colonies selected from PCR: XL-10 Gold cells were cultivated in 4 ml of LB supplemented with kanamycin (50 µg/ml) on a shaker at 120 rpm for 15 hours at 37°C.

DNA extraction was performed using QIAprep Spin Miniprep Kit (Qiagen, #27106) following the manufacturer's protocol. The absorbance, A260, and the ratio A260/A280 parameters of extracted DNA were quantified with the nanodrop (company, cat no) and the extracted DNA was sent to Eurofins Genomics to be sequenced.

Successfully inserted colonies were then amplified in 300 ml LB supplemented with kanamycin (50 µg/ml) for 15 hours at 37°C on a shaker at 120 rpm.

DNA extraction of bacteria harvested in maxi culture was performed with PureLink™ HiPure Plasmid Filter Maxiprep Kit (Invitrogen, #K210017) according to the manufacturer's protocol, except for the performed temperature, which was changed from RT to 4°C. The absorbance, A260 and A260/A280 parameters were quantified with the nanodrop.

6.4 Transfection

On the first day, U2OS cells were seeded on the plates specified in the table according to the method to be performed:

experiment	plate	Number of cells seeded in each well
Immunofluorescence (seeded on φ18 mm coverslips)	12-well plate, SARSTEDT, #83.3921.500	30 000
High throughput imaging analysis	96-well half area plate for imaging Greiner Bio-One, 675090	3000
Western blot and flowcytometry	6-well plate, SARSTEDT, #3022921	60 000

On the second day, the medium has been changed with 80% of the seeding volume from complete DMEM to antibiotics-free DMEM and the cells have been transfected for 48 hours according to the following set up:

	DNA (µg/well)	Transfection reagent	Ratio transfection reagent (µl)/DNA (µg)
immunofluorescence	0.24	Lipofectamine 3000 Thermo Fisher Scientific, #L3000015	2:1
High throughput imaging analysis	0.1		
Western blot	0.5		
flowcytometry	0.3	PEI MAX tebu bio # NC1038561	10:1

DNA was diluted to the desired concentration in TE Buffer (Invitrogen #00866039). Transfections with lipofectamine reagents were performed diluting DNA and p3000 together in Opti-MEM I Reduced Serum Medium (Gibco, #31985070) and lipofectamine 3000 in Opti-MEM in separated tubes. After 5 minutes of incubation at RT, the lipofectamine dilution was added to the DNA mix. After 20 minutes, the final solution was poured to the corresponding well. As for transfection with PEI MAX: 0.1 ng of DNA and 1 µl of PEI were diluted in 100 µl of Opti-MEM and incubated for 15 minutes at room temperature before the solution was poured in each well. On the third day, the medium was changed from DMEM without antibiotics to the complete DMEM for each well.
On the fourth day, the transfected cells were analyzed or harvested following each protocol.

6.5 Western blotting

U2OS cells were seeded on a 6 well plate and transfected for 48h. Full protein lysate was extracted from U2OS cells. Cells were rinsed with 1X phosphate-buffered saline (PBS) and scraped with cell scraper on ice. Collected cells have been centrifuged at 1200 xg for 5 minutes at 4°C. The pellet was treated with 100µl of cell lysis buffer (HEPES 5 x 10^-3M PH 7.5, NaCl 0,015 M, 1,5 x 10^-4 M $MgCl_2$, EGTA 1 x 10^-4 M , Triton 100X 0,1 %, glycerol 1%,) supplemented with complete Easy protease inhibitor cocktail tablets from Roche and 1M NaF and 0,1M Na_3VO_4 for each condition. The samples were centrifuged at 13000 xg for 15 min at 4°C and the supernatant was collected as whole cell lysate. Protein concentration was determined using Pierce BCA Protein Assay Kit (Thermo Scientific) and lysates were diluted to desired concentrations with the 2X cell lysis buffer. To perform a denaturing LDS PAGE, samples were prepared using a solution of 87,5% of NP0008 Invitrogen™ NuPAGE™ LDS Sample Buffer (4X)

and 12,5% of β -mercaptoethanol (SIGMA). Protein samples were incubated at 70°C for 10 min in the heat block. To perform electrophoresis, the samples were loaded on SurePAGE, Bis-Tris, 4-20% gels (#M00655 GenScript) and ran in 1X Tris-MOPS-SDS Running Buffer (#M00138 GenScript) for 15 min at 90 V and then for 90 min at 120 V. After electrophoresis, proteins were transferred onto PVDF Transfer Membranes (Thermo Fisher Scientific #88518) in transfer buffer (6g TRIS, 28,8g glycine, 400mL methanol and milliQ till 2L) by applying a constant current of 200 mA for 75 min at 4°C. The membrane was then incubated in blocking buffer (3% Bovine serum albumin (BSA) in TBST (Tris buffered saline 1x supplemented with 0.05% Tween 20) for 30 min at RT and proteins were probed overnight at 4°C using primary antibodies in 3% BSA (1:1000). After the incubation the membranes were washed 3 times in TBST for 30 minutes and incubated for 1 hour with the secondary antibody. After the incubation the membranes were washed 3 times in TBST 1x and developed in iBright Imaging Systems Features by Thermo Fisher scientific. Protein expression was detected with Immobilon Crescendo Western HRP (Sigma-Aldrich, #WBLUR0100) or Immobilon Forte Western HRP substrate (#WBLUF0500). The following antibodies were used for Western blotting:

Primary antibody	Secondary antibody
HA-Tag (C29F4) Rabbit mAb #3724 by Cell Signaling Technology	HRP-conjugated Goat anti-Rabbit IgG (H + L) 926-80011 Li Cor #D10601-03
c-Myc Monoclonal Antibody (9E10) by Thermo Fisher	HRP-conjugated Goat anti-Mouse IgG (H + L) 926-80010 Li Cor #D10409-04
Anti-α-tubulin monoclonal clone B-5-1-2 #T5168 Sigma-Aldrich	

6.6 Immunofluorescence

Probes localization was assessed through immunofluorescence. On the first day 30 000 U2OS cells in 1ml of complete DMEM were seeded on 24mm coverslips for each well in TC-PLATTE 12 Well, Standard, F SARSTEDT AG & Co. KG. U2OS cells were transfected following the transfection protocol described above. The fourth day cells were fixed for 10 minutes in 4% paraformaldehyde, washed 3 times in PBS 1x and stored at 4°C. After fixation cells were permeabilized adding 300µl of 0.1% tritonX100/PBS in each well for 10 minutes. At the end of the incubation U2OS were washed 3 times with PBS 1x and incubated for 30 minutes with blocking solution (3%BSA/PBS). After 30 minutes the coverslips were mounted on the corresponding primary antibody solution (1:500 dilution in BSA) and incubated for 60 minutes. After 60 minutes the coverslips were washed 3 times with PBS 1x and mounted on the secondary antibody solution (1:500 dilution in BSA) for 60 minutes. After 60 minutes the coverslips were washed 3 times with PBS 1x and mounted on glass slides using ProLong™ Glass Antifade

Mountant #P36980 by Invitrogen which was left to solidify over night at 4°C in the dark. All the incubation steps were performed at room temperature in the dark. U2OS cells were imaged using a ZEISS LSM 900 confocal microscope with a Plan-Apochromat 63x/1.4 Oil DIC M27 420782-9900-000 Objective. The acquisition was performed using ZEN BLUE and the following laser set up:

	excitation	emission
Track 1	AF647	637nm-700nm
Track 2	AF568	563nm-620nm
Track3	AF488	486nm-570nm

Master gain was kept at 800V, digital offset: 0, digital gain: 1.0, pin hole: 58µm. The acquired images were processed using ImageJ software. The following antibodies were used for immunofluorescence:

Primary antibody	Secondary antibody
Anti-SDHA Invitrogen 459200 Mouse IgG	Rabbit anti-Mouse IgG (H+L) Cross-Adsorbed Secondary Antibody, Alexa Fluor™ 647 # A-21239 by Thermo Fisher scientific
Anti-calnexin in rabbit -IgG fraction of antiserum, buffered aqueous solution #C4731 by Sigma-Aldrich	Donkey anti-Rabbit IgG (H+L) Highly Cross-Adsorbed Secondary Antibody, Alexa Fluor™ 647 #A31573
HA-Tag (C29F4) Rabbit mAb #3724 by Cell Signaling Technology	Donkey anti-Rabbit IgG (H+L) Highly Cross-Adsorbed Secondary Antibody Alexa Fluor™ 568 #A10042
c-Myc Monoclonal Antibody (9E10) by Thermo Fisher Scientific	Anti-Mouse IgG H&L (Alexa Fluor® 488) °A21202 by Life technology
Tom20 (D8T4N) Rabbit mAb #42406 by Cell Signaling Technology	Goat anti-Rabbit IgG (H+L) Cross-Adsorbed Secondary Antibody, Alexa Fluor™ 488 #A11008 by Invitrogen Goat anti-Rabbit IgG (H+L) Cross-Adsorbed Secondary Antibody, Alexa Fluor 647 #A31573 Goat anti-Rabbit IgG (H+L) Cross-Adsorbed Secondary Antibody, Alexa Fluor™ 568 #A10042

6.7 High throughput imaging analysis

U2OS cells were seeded and transfected according to the protocols described above. On the fourth day, the medium of each well was changed to 15µl of

imaging medium. Imaging medium is based on DMEM without phenol red (Sigma-Aldrich D5030) supplemented with 0.25% of FBS, 1% of PSG (Gibco, #10378-016), NEAA (Gibco#11140050,), pyruvate (Gibco, #11360070), 0.37% of NaHCO3 and 0.45% of glucose. Treatment with 1 mM of TF-CORAL (Twinkle-factory #516600-250) was performed to each well immediately before imaging.
Imaging was performed using an Operetta CLS High Content Analysis System (Perkin Elmer). The images were acquired using a 40X, 1.1N.A. objective in non-confocal mode. The ROI was 2160 x 2160. Detector channels were set up according to the following parameters:

		excitation-emission wavelength	Exposure Time	Power
Channel 1	Brightfield		20 ms	10%
Channel 2	Coral	516-600 nm	100 ms	50%
Channel 3	CFP	435-477 nm	10 ms	40%

Images were post-processed and analyzed through ImageJ.

6.8 Flow cytometry

U2OS cells were harvested from 2 wells of 6-well plate for each condition, as following. U2OS were rinsed in PBS 1x, trypsinized (300 µl for each well, 3 minutes at 37°C) and centrifuged at 600 xg for 5 minutes at 4°C. The pellets were resuspended in 300 µl of FCM buffer (PBS 1x, 5 mM EDTA, 25 mM HEPES (pH 7.0), 1% albumin) at 4°C.
We performed flowcytometry using a BD FACSCanto™ II System (BD Biosciences) in HTS mode. The Blue 488 nm laser at was used in combination with 585/42 filter (PE) to detect the fluorescent derived from FAST-Coral complex, while the 405 nm Violet laser in combination with 450/50 filter (BFP) was used to detect mTagBFP2. The compensation was kept at 0%, verified with single-color-stained controls, and samples were loaded according to the following set up:

Sample flow rate (µl/sec)	1.0
Sample volume (µl)	10
Mixing volume (µl)	25
Mixing speed (µl/sec)	100
Number of mixes	3
Wash volume (µl)	400

The results were post-processed through FCSalyzer software (version 0.9.22 alpha, https://sourceforge.net/ projects/fcsalyzer/). The efficiency of coral fluorescent signal was assessed as the percentage of PE positive cells in BFP positive cells.

CHAPTER 7: RESULTS

7.1 Design of STACCATO probes

In this Thesis work we generated and characterized STACCATO, a Split-FAST Mitochondria-ER Contacts probe. STACCATO is intended for MERCs visualization. STACCATO is based on the specific targeting of the C-FAST and N-FAST moieties of Split-FAST to the outer mitochondrial membrane and to the surface of the ER, respectively. When cells are perfused with the fluorogen and the two moieties are close enough, STACCATO is reconstituted and becomes fluorescent, allowing in principle the visualization and quantification of MERCs (Fig. 1).

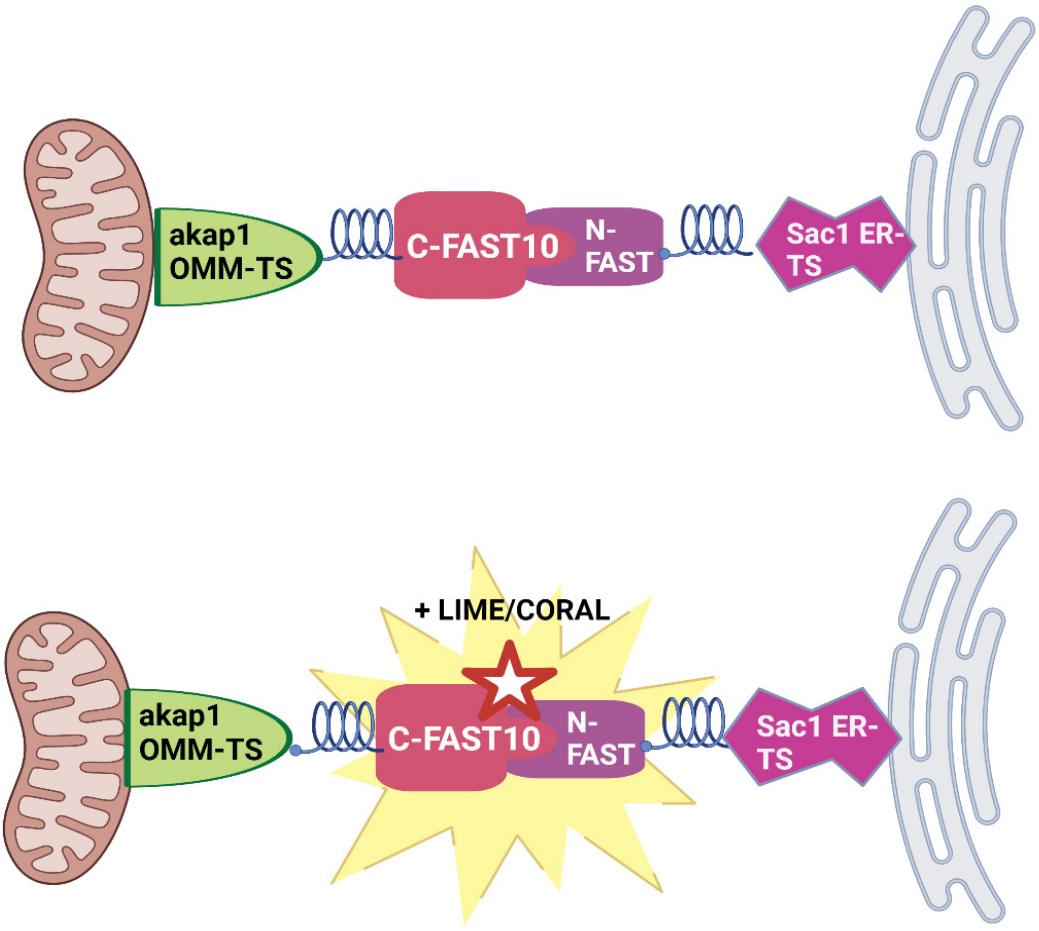

Figure 1 Schematic representation of mechanism of STACCATO reconstitution. STACCATO with OMM-targeted C-terminus FAST and ER-targeted N-terminus FAST reconstitute and fluoresce at the MERCs upon addition of the fluorogen: Lime (480-541nm) or Coral (516-600nm)

The STACCATO probes have been originally designed by Dr. S. Shinjo in different versions, with 6 different C-FAST targeted to the mitochondria and 3 N-FAST targeted to the surface of the ER. The different C- and N-FAST moieties targeted to the two organelles differ for the length of the linked between the

organelle anchor and the FAST domain. This modular design allows the different versions to be combined so that the experimenter can in principle detect MERCs characterized by a few nanometers' width (~0-3 nm) up to very wide, ~30 nm MERCs. In addition, we prepared STACCATO versions that differ in their C-FAST moiety, bearing the C-FAST10 or the C-FAST11 halves of the Split-FAST probe. Such a design allowed us to capitalize on the different K_D of the C-FAST10 and the C-FAST11 with N-FAST, thus allowing to generate STACCATO probes with predicted differential reversibility parameters.
To generate a probe that can measure MERCs of different widths, we designed an array of STACCATO probes characterized by different linkers between the organelle anchor and the C- and N-FAST. We designed a "short" STACCATO, where the organelle anchor is connected to the C-FAST10, C-FAST11 and N-FAST without a rigid linker (we refer to these STACCATO halves as short C- and N-FAST). Such a design allows to reconstitute a short-STACCATO probe that in principle spans MERCs as small as the size of C-FAST plus that of the N-FAST portion of the probe (~2nm).We also designed a medium STACCATO, where C-FAST10, C-FAST11 and N-FAST are connected by a linker of 7 nm (predicted to be rigid by AlphaFold2), allowing to measure MERCs up to ~16 nm. Finally, we designed a long STACCATO, where C-FAST10, C-FAST11 and N-FAST are connected by a linker of 14 nm (again predicted by AlphaFold2 to be rigid) to the organelle anchor. Long STACCATO can measure up to ~30 nm wide MERCs

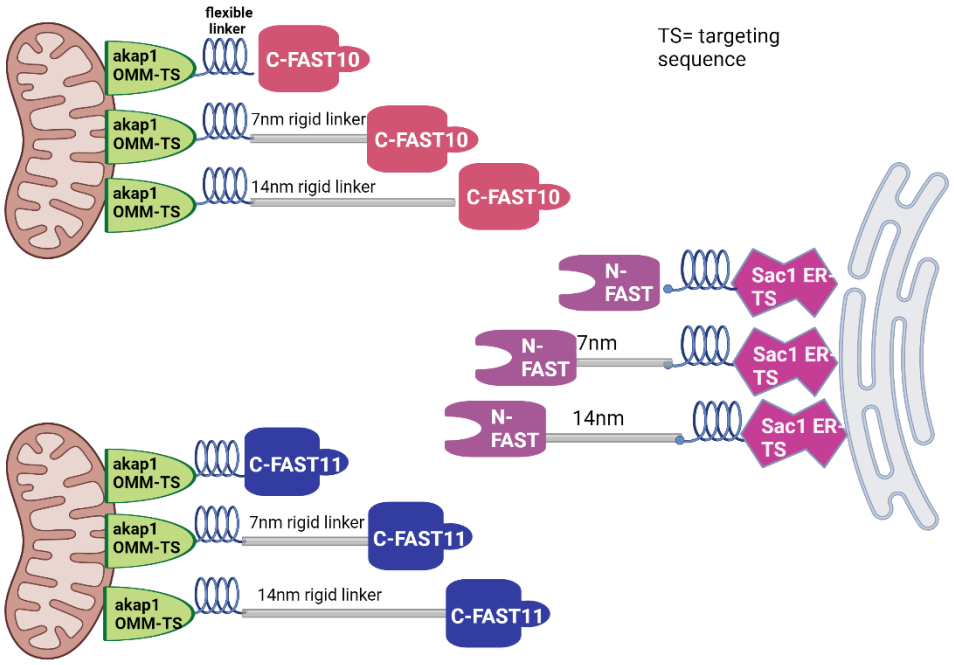

Figure 2 Schematic representation of short, medium and long STACCATO probes. We designed 6 mito-targeted with 3 ER-targeted probes of different lengths. The short pair is the association of the C-FAST and N-FAST lacking rigid linkers, while the longer is made the association of C-FAST and N-FAST with 7 or 14 nm rigid linkers to detect MERCs of width from ~2 to ~30 nm.

(Figure 2). Because the rigid linkers are connected to the anchors by a flexible linker, in principle the different medium and long C-FAST10, C-FAST11 and N-FAST can orient themselves with different angles on the surface of the organelles. This means that the probes do not generate a steric hindrance at the interorganelle space and that they can measure MERCs from 2 nm (the size of the reconstituted Split-FAST) to 16 (in the case of medium STACCATO) or to 30 nm (in the case of long STACCATO). Because in principle all the different halves can be combined as desired, the design of STACCATO allows to measure a wide range of MERCs distances, with a lower limit defined by the hindrance of the reconstituted SplitFAST protein and an upper limit defined using the two long N- and C-FAST moieties (Fig. 2).

7.2 Generation of short, medium and long STACCATO probes and expression in U2OS cells

We cloned C-FAST10, C-FAST11 and N-FAST with short, medium, and long linkers in a mammalian expression plasmid (pSIK). Following confirmation by sequencing of the correct sequences of the cloned plasmids, we used them to transfect U2OS cells.

To determine if U2OS cells transfected with the probes express the full protein according to their predicted molecular weight (MW), Western blotting was performed. We cloned the probes so that the mitochondrially targeted moieties contain an HA-tag between the linkers and the C-FAST, while ER-targeted probes contain a Myc-tag between the N-FAST and the linker. To detect the N-FAST probe, we used an anti-Myc primary antibodies. While these experiments confirm that N-FAST moieties are correctly expressed, the N-FAST moieties tested here display a double band pattern (Fig. 3A). The MW of the upper bands appearing in

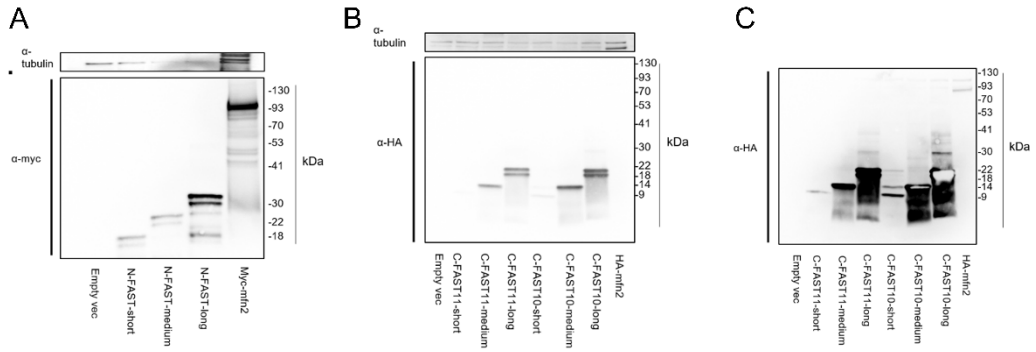

Figure 3 Immunoblot detection of C- and N-FAST moieties of STACCATO in U2OS cells. U2OS cells were transfected with the indicated plasmids and after 48 h cells were lysed. Equal amounts of proteins from total lysates (20µg) were separated by SDS-PAGE, transferred to PVDF membranes, and incubated with the anti-Myc (A) or anti HA (B,C) antibodies. (B) short and (C) long exposure of anti HA incubated membranes. In panels A and B membranes were also incubated with antibodies against tubulin as a loading control.

cells transfected with N-FAST corresponds to the expected MW of these probes (Table 4). The lower MW bands might correspond to proteolytically cleaved forms of the N-FAST, or to posttranslational modifications (see discussion). To

detect the C-FAST proteins, Western blot against the HA tag was performed on whole cell lysate of U2OS cells transfected with C-FAST probes and HA-MFN2. The HA signal appeared upon a short exposure of the membranes containing lysates from the cells transfected with the medium and long C-FAST probes (Fig. 3B). The HA signal appeared upon longer exposure of the membranes containing lysates from cells transfected with short C-FAST or HA-MFN2 (Fig. 3C).

C-FAST11-short	10.5 kDa
C-FAST11-medium	15.2 kDa
C-FAST11-long	20.2 kDa
C-FAST10-short	10.4 kDa
C-FAST10-medium	15.1 kDa
C-FAST10-long	20.1 kDa
N-FAST-short	22.8 kDa
N-FAST-medium	27.5 kDa
N-FAST-long	32.5 kDa

Table 4. Predicted MW of the expressed STACCATO moieties. Data are calculated from the nucleotide sequence of the probes.

In conclusion, these Western blot experiments confirm that the probes are correctly expressed in a human cell model.

7.3 STACCATO probes moieties are correctly targeted to mitochondria and ER.

STACCATO is based on the reconstitution of a split probe with its C-terminus localized to the OMM and N-terminus localized to the ER membrane. C-FAST probes have a mito-targeting signal derived from AKAP1 while N-FAST probes possess an ER-targeting signal derived from Sac1.
To test whether C-FAST probes effectively localize to mitochondria and N-FAST probes localize to the ER, we performed immunostaining and imaging with confocal microscopy. To determine if C-FAST probes localize to mitochondria, we transfected U2OS cells with C-FAST and matrix-targeted mitoYFP and we performed immunostaining for C-FAST, and endogenous SDHA. Visualization of immunostained U2OS cells at the confocal microscope indicated that C-FAST probes colocalize with mitoYFP and SDHA (Fig. 4A-B). We observed that part of the mitoYFP signal was retrieved in the nucleus and in the cytosol, suggesting that mitochondrial protein import could be impaired in cells transfected with C-FAST probes. Mitochondria in C-FAST transfected cells appear fragmented compared to mitochondria of cells transfected with empty vector (not shown), suggesting that C-FAST might alter mitochondrial morphology. On the other hand, in cells transfected with C-FAST10-long probe mitochondrial morphology was comparable to that observed in empty vector transfected cells, suggesting that this

STACCATO moiety does not affect mitochondrial morphology. These results indicate that the probes correctly localize at mitochondria, but further tests are required to verify if they localize on the OMM.
To determine if N-FAST moieties localize to ER, we transfected U2OS cells with ER-membrane-targeted mCherry (Sec61beta-mCherry) and N-FASTs, and we performed immunostaining for N-FAST and for the endogenous ER marker calnexin. Confocal microscopy of immunostained U2OS cells indicated that the N-FAST probes colocalize with the ER markers mCherry and calnexin. N-FAST probes efficiently decorate the ER network, without causing apparent changes in its morphology as compared to U2OS cells transfected with empty vector. (Fig. 4C).

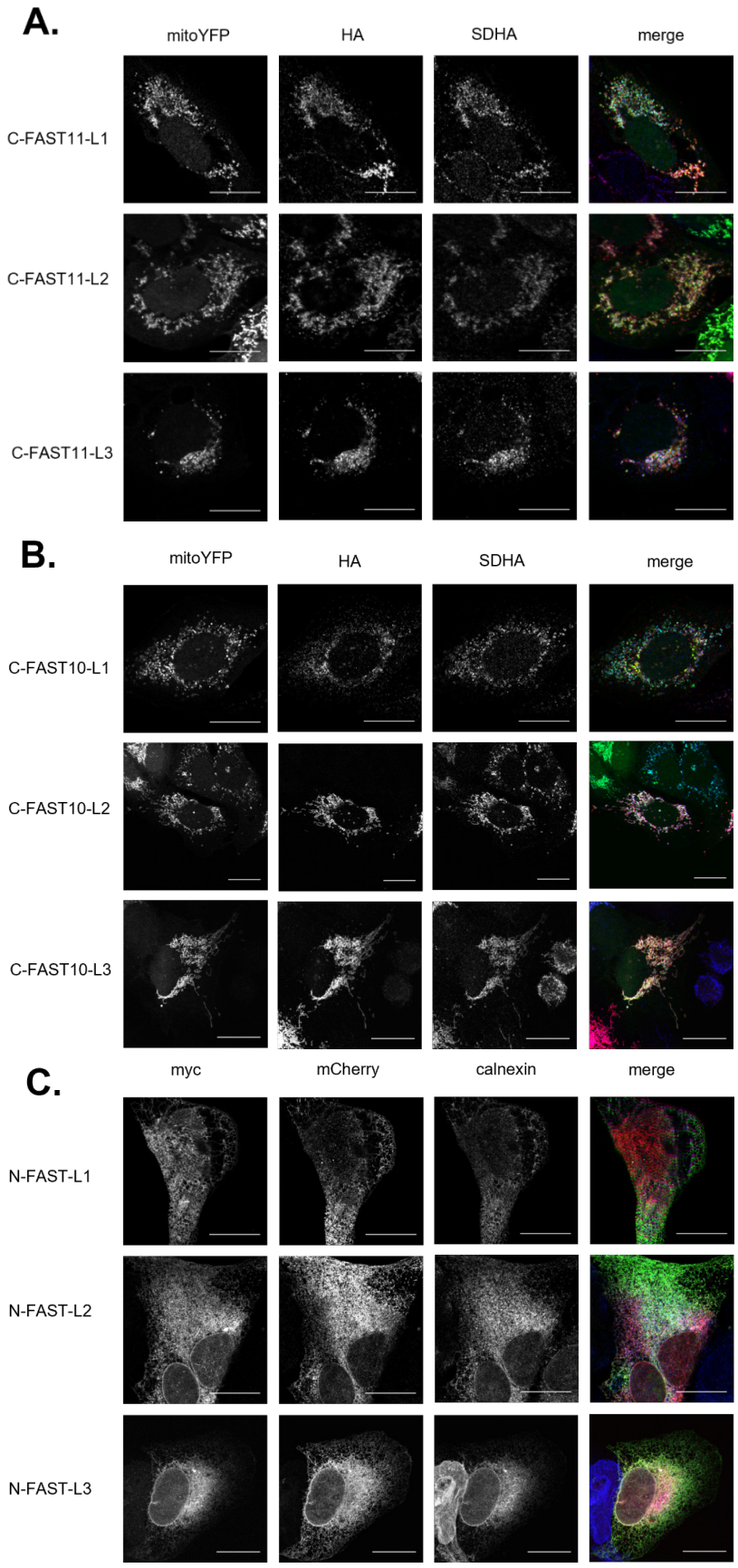

Figure 4 Immunofluorescence detection of C- and N-FAST moieties of STACCATO in U2OS cells. (A-C). Representative confocal images of U2OS cells cotransfected with C-FAST and mtYFP (A,B) or N-FAST and Sec-mCherry (C), fixed and immunostained with the indicated antibodies. In A,B the merged images, green, red, and blue indicate mitoYFP, HA and SDHA. In C, green, red and blue indicate N-FAST, mCherry and calnexin. The scalebars are 20µm.

7.4 Validation of STACCATO through high throughput imaging and flow cytometer analysis.

7.4.1 High throughput imaging

C-FAST and N-FAST, coexpressed in the same cell, emit fluorescence when they are proximal enough to be reconstituted upon addition of cell permeant fluorogen (Coral) to the cell medium. To determine whether the pairs of STACCATO probes emit fluorescence upon Coral treatment, we used a high throughput imaging system (Operetta CLS).

First, we confirmed that the cells transfected with mitoFAST display a mitochondria-localized fluorescent signal upon Coral perfusion, suggesting successful Coral-FAST reconstitution and detection in U2OS cells. We therefore decided to test all the possible combinations of N-FAST and C-FAST STACCATO moieties in U2OS cells co-transfected with mitoCFP to identify the transfected cells. The cells transfected with the different STACCATO pairs seldom displayed fluorescence upon perfusion with Coral, especially in cells that

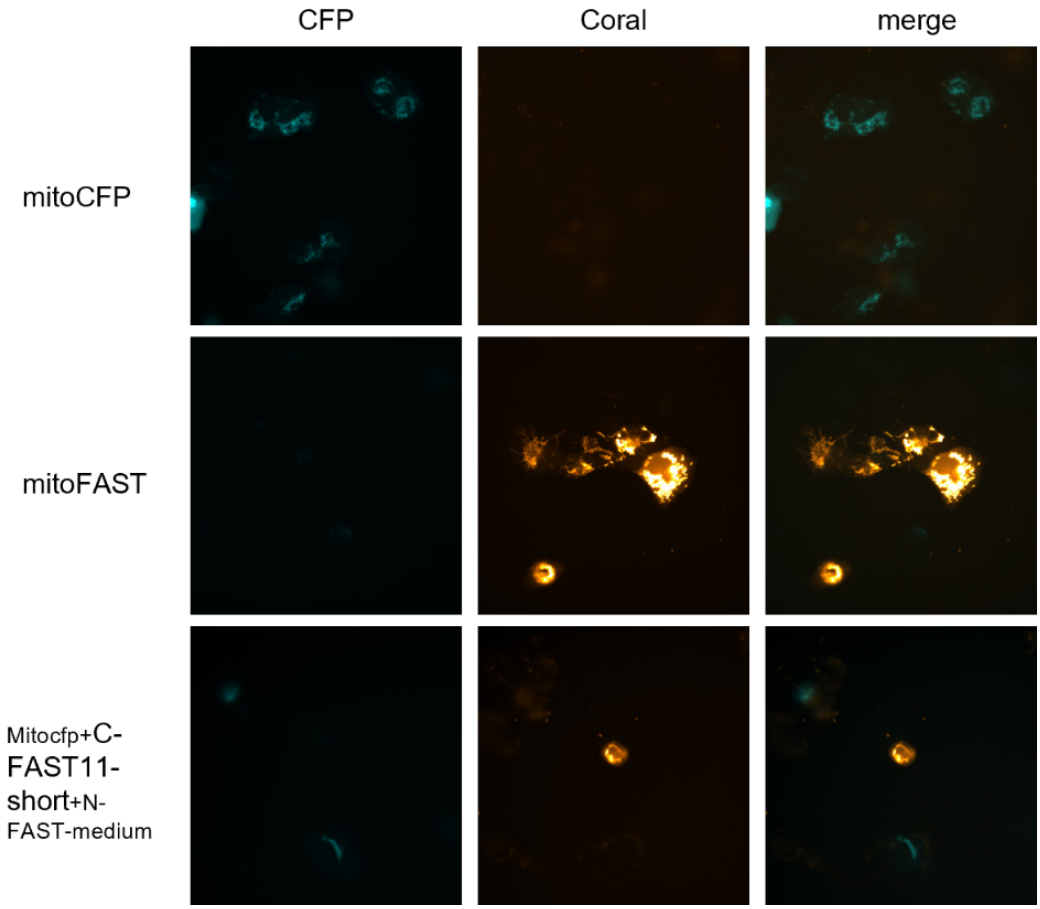

Figure 5 ***High throughput imaging of mitoCFP; mitoFAST and STACCATO in transfected U2OS cells***. All combinations of C-FAST and N-FAST were cotransfected with mitoCFP and observed at Operetta CLS. Images for each condition were acquired before treatment and after treatment with Coral. Representative images of cells in CFP channel detection are shown in cyan; cells in Coral channel detection are shown in orange; the merge of the two channels is shown in cyan and orange. In mitoCFP+C-FAST11-short+N-FAST-medium merge there are Coral positive, mitoCFP+ cells.

appeared round or dying (Figure 5). These results were independent of the STACCATO moieties (C-FAST10 or C-FAST11) and length (short, medium, long) used. These results suggest that the expression of STACCATO is toxic for the cells or that the N- and C-FAST cleavage detected upon expression of the probe can reduce the propensity of STACCATO to reconstitute.

7.4.2 Flow cytometry

Because of the slim success of the probe in the HCI setting, we decided to test if it was sufficient to identify MERCs in single cells analyzed by flow cytometry. In this case, we decided to coexpress with STACCATO a mitoBFP or mitoBFP-tether, which induces artificial tethering of MERCs (Hirabayashi et al., 2017), to determine if STACCATO displays an increase in population of Coral positive cells in MERCs-tethered conditions. This approach guarantees that we detect the fluorescence of STACCATO only in BFP positive, successfully transfected, singlet alive cells. Indeed, flow cytometry is more sensitive than microscopy and it allows to detect even low fluorescence. Moreover, it allows to exclude from the analysis auto fluorescent dying cells, cell clusters or fluorogen aggregates. We tested several pairs of the probes: short C-FAST and N-FAST, medium C-FAST and N-FAST, long C-FAST and N-FAST or long C-FAST with short N-FAST. The results from flowcytometry analysis indicated that the number of cells displaying Coral fluorescence increased when cells transfected with short,

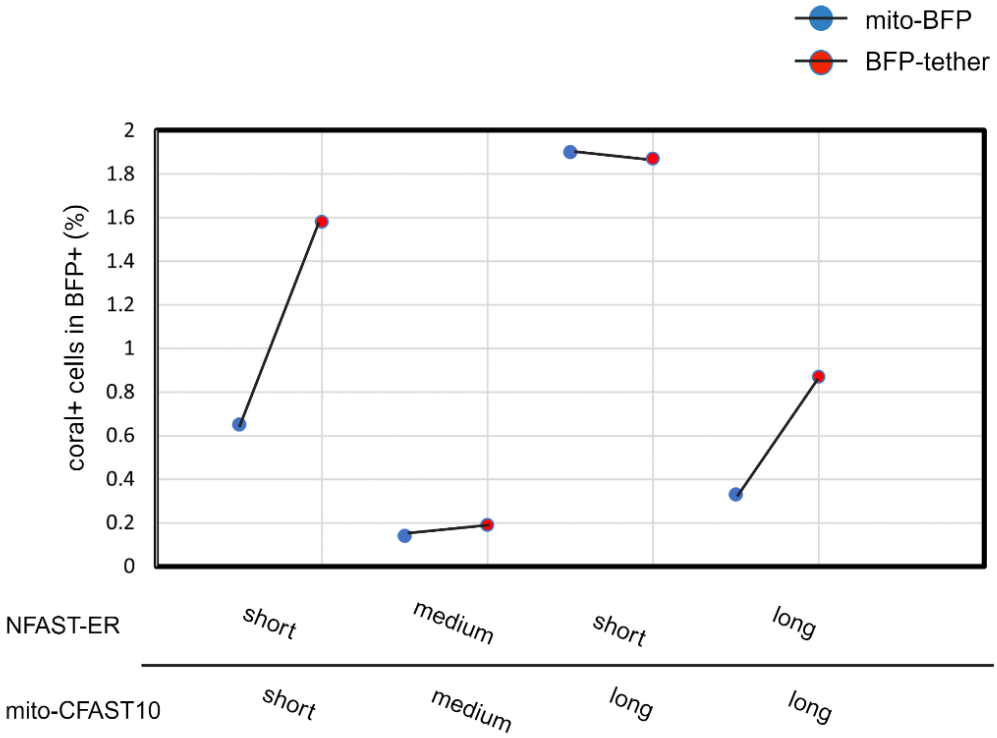

Figure 6 Flowcytometry analysis on STACCATO-cotransfected cells. Percentage of Coral+ cells in the BFP+ U2OS cells cotransfected with the indicated STACCATO pairs and the indicated BFP containing plasmid.

medium and long STACCATO coexpressed the mitoBFP-tether compared to the control mitoBFP coexpressing cells. This result was not observed when cells expressed the long C-FAST and the short N-FAST and was marginal when cells express the medium C- and N-FAST pair (Figure 6). Thus, short and long STACCATO pairs can report changes in ER-mitochondria proximity induced by an artificial tether, at least in flow cytometry.

CHAPTER 8: DISCUSSION

In eukaryotes, cellular organelles are delimited by membranes. The organelles can come in contact through sites of proximity between their membranes: the membrane contact sites (MCSs) which are physically and functionally unique compartments of the cells. The most well characterized and studied membrane contact site is the one between mitochondria and ER (MERCs). A whole new field is emerging to investigate the rules that govern these sites and how they impact or are affected by cellular state. The term "MERCs" is used to describe sites of physical apposition between mitochondria and ER where resident and transient proteins perform specific functions. The term "MAMs" is used to refer to the proteome and the biochemical nature of the MERCs. MERCs and MAMs are highly dynamic: the number of contacts between the two organelles and the proteome changes according to the pathophysiological state of the cell. In particular, MERCs increase in stress conditions and their width corresponds the optimal distance to perform the function required. MAMs proteome comprises tethering, functional, sorter and regulator proteins. MAMs are the platform for ion exchange between ER and mitochondria; in particular apoptosis induction depends on the regulation of Ca^{2} in this contact site. MAMs are the site of synthesis of triacylglycerol, phospholipids and steroid hormones and engage in mitochondrial fission and fusion dynamics.

MAMs research field is developing new techniques to characterize these sites and to visualize them. The techniques currently in use to study MAMs proteome comprise proximity labeling assays, pull down, fractionation, while for their visualization electron microscopy and confocal microscopy are employed. MERCs can be highlighted at confocal microscopy through Föster resonance energy transfer (FRET), bimolecular fluorescent complementation (BiFC) and dimerization-dependent fluorescent proteins (ddFP). These tools present several pitfalls: probes' interactions required in ddFP and FRET to detect MERCs have high dissociation constants, this decreases the probability of irreversible interactions and, in turn, artificial tethering, but is correlated to low signal emission. BiFC, on the other hand, displays a high signal to noise ratio, but the molecular complementation of the probe requires interactions of low dissociation constants, increasing the risk of irreversible interactions in the split-reporter and of artificial formation of new contact sites.

In this Thesis, we analyze a split fluorescent reporter that could be used as an alternative to the tools described above. This probe, that we dubbed "STACCATO", is designed on the basis of the splitFAST, a probe developed by Tebo and Gautier in 2019. SplitFAST is designed to retain the properties of FAST, a probe designed in 2015 by the same group and able to show a high S/N ratio immediately upon reversible binding with a cell permeant fluorophore. STACCATO has been designed to emit fluorescence upon reconstitution of the C-FAST moiety targeted to the outer mitochondrial membrane together with the N-FAST moiety targeted to the ER membrane in the presence of the fluorogen. The

reconstitution of the probe is immediate and completely reversible. Here we tested 6 probes targeted to the mitochondria (C-FAST10/ C-FAST11) and 3 probes targeted to the ER (N-FAST). C-FAST10, C-FAST11 and N-FAST are designed in 3 versions, one equipped without a flexible linker (short), one equipped with a short rigid linker (7 nm) and one with a long rigid linker (14nm). The pair of probes can be reconstituted at the MERCs as wide as the FAST fragments can reach to each other, which means the long linker pairs can cover the MERCs from 2-3 nm to 30 nm.

The probes were realized through molecular cloning. The sequencing of plasmids confirmed that we were able to obtain all the designed probes. Through Western blot on total cell lysate of transfected cells, we were able to corroborate that C-FAST-short and C-FAST-medium are expressed in the cell with the expected molecular weight. C-FAST-long in Western blot display double bands: the upper band corresponds the expected molecular weight of the probes, while the lower bands correspond a molecular weight that is 10% inferior to the expected molecular weight of these probes. Through Prop – 1.0 by Department of Health Technology, Technical University of Denmark (https://services.healthtech.dtu.dk/services/ProP-1.0/), we found that all C-FAST probes present a serine-arginine-lysine (SRK-KD) domain at residue 29th which can undergo post translational cleavage. C-FAST have a transmembrane domain comprised between the amino acid from 7th to 26th residue and through the recognition of this domain by the sorting and assembly machinery (SAM) complex they are integrated in OMM, after they have been imported by translocase of the outer membrane (Tom) complex (Höhr et al., 2015). It is possible that the length of C-FAST-long probes cause them to be overcome in Tom and translocase of the inner membrane (Tim) complex, exposing the residues from 1 to 29 to the matrix where they are cut by mitochondria processing peptidases (MPP) (Kunová et al., 2022). This mechanism can explain why the observed MW of long C-FAST is lower than the expected one and why this happens for some but not all C-FAST-long probes. New probes can be designed which can be equipped with rigid linkers of length inferior to 14 nm, or the SRK cleavage site can be easily mutagenized. N-FAST-short, N-FAST-medium and N-FAST-long all appear as a doublet in Western blot. The expected MW of N-FAST-short -medium and -long corresponds to the upper bands retrieved upon immunoblotting. These probes do not possess a serine-arginine-lysine cleavage site, complicating the correction of their unexpected cleavage.

Visualization at confocal microscope of U2OS cotransfected with SDHA, mitoYFP and C-FAST probes and immunostained for SDHA and C-FAST showed that C-FAST probes localize at mitochondria. MitoYFP is targeted to the mitochondrial matrix, but a mitoYFP signal was detected in the nucleus of U2OS cells. Protein import in mitochondrial matrix is dependent on the membrane potential across the inner membrane, so the detection of a mitoYFP signal in the nucleus could suggest that the mitochondrial membrane potential of U2OS cells

transfected with C-FAST is reduced (Martin et al., 1991). In order to test whether the membrane potential is reduced upon the expression of C-FAST, potentiometric dyes such as TMRM can be used. Moreover, we noticed that C-FAST expressing mitochondria were fragmented compared to the control (not shown). To assess if C-FAST affects mitochondria homeostasis or if mitochondria appear fragmented because subjected to the stress of cotransfection, it would be useful to perform co-localization experiment at confocal microscope with U2OS cells stably expressed with mitoYFP.
Visualization at confocal microscope of U2OS cotransfected with calnexin, Sec61beta-mCherry and N-FAST probes and immunostained for calnexin and N-FAST showed that N-FAST probes localize at ER. N-FAST efficiently decorates the ER without altering its morphology.
Imaging at Operetta and flow cytometry analysis showed that fluorescent emission signal of probes is very weak to be detected with confocal microscope. Through flow cytometry, we show that short and long STACCATO respond to the expression of an artificial tether with the expected increase in fluorescence. Further studies using flow cytometry are required to identify pairs that give the higher percentage of Coral positive cells.
After testing all the possible combinations, STACCATO can be improved to increase the percentage of Coral positive cells. One possibility would be to generate single plasmids expressing the N- and C-FAST moieties of interest intercalated by a 2A self cleavable system. Moreover, the use of a viral delivery system can increase of course the efficiency of expression. The 2A peptide is an amino acid sequence that undergoes self-cleavage and exon skipping with the formation of glycyl-prolyl peptide at its C-terminus. Such a system could increase the population of Coral positive cells, because it would guarantee cotransfection and more importantly the equimolar expression of C-FAST and N-FAST.
Once optimized, the STACCATO system can be used to visualize and define MERCs width according to the state of the cell. A probe that is able to highlight different widths of MERCs can be used to assess which width of the MERCs have function or is affected in physiological/pathological context. STACCATO could be used to determine differences in MERCs widths between a healthy and a cell in specific pathological conditions. In this way it would be possible to identify the players involved in changes of widths, to understand the dynamics of width change and to target it in treatments aimed at rescuing cell homeostasis.

BIBLIOGRAPHY

Abrisch, R. G., Gumbin, S. C., Wisniewski, B. T., Lackner, L. L., & Voeltz, G. K. (2020). Fission and fusion machineries converge at ER contact sites to regulate mitochondrial morphology. *Journal of Cell Biology*, *219*(4). https://doi.org/10.1083/jcb.201911122

Alford, S. C., Abdelfattah, A. S., Ding, Y., & Campbell, R. E. (2012). A Fluorogenic Red Fluorescent Protein Heterodimer. *Chemistry & Biology*, *19*(3), 353–360. https://doi.org/10.1016/j.chembiol.2012.01.006

Alford, S. C., Ding, Y., Simmen, T., & Campbell, R. E. (2012). Dimerization-Dependent Green and Yellow Fluorescent Proteins. *ACS Synthetic Biology*, *1*(12), 569–575. https://doi.org/10.1021/sb300050j

Anastasia, I., Ilacqua, N., Raimondi, A., Lemieux, P., Ghandehari-Alavijeh, R., Faure, G., Mekhedov, S. L., Williams, K. J., Caicci, F., Valle, G., Giacomello, M., Quiroga, A. D., Lehner, R., Miksis, M. J., Toth, K., de Aguiar Vallim, T. Q., Koonin, E. V., Scorrano, L., & Pellegrini, L. (2021). Mitochondria-rough-ER contacts in the liver regulate systemic lipid homeostasis. *Cell Reports*, *34*(11), 108873. https://doi.org/10.1016/j.celrep.2021.108873

Balla, T. (2013). Phosphoinositides: Tiny Lipids With Giant Impact on Cell Regulation. *Physiological Reviews*, *93*(3), 1019–1137. https://doi.org/10.1152/physrev.00028.2012

Banaszynski, L. A., Liu, C. W., & Wandless, T. J. (2005). Characterization of the FKBP·Rapamycin·FRB Ternary Complex. *Journal of the American Chemical Society*, *127*(13), 4715–4721. https://doi.org/10.1021/ja043277y

Bastiaens, P. I., Majoul, I. V., Verveer, P. J., Söling, H. D., & Jovin, T. M. (1996). Imaging the intracellular trafficking and state of the AB5 quaternary structure of cholera toxin. *The EMBO Journal*, *15*(16), 4246–4253. https://doi.org/10.1002/j.1460-2075.1996.tb00799.x

Bernhard, W., & Rouiller, C. (1956). CLOSE TOPOGRAPHICAL RELATIONSHIP BETWEEN MITOCHONDRIA AND ERGASTOPLASM OF LIVER CELLS IN A DEFINITE PHASE OF CELLULAR ACTIVITY. *The Journal of Cell Biology*, *2*(4), 73–78. https://doi.org/10.1083/jcb.2.4.73

Berridge, M. J. (2016). The Inositol Trisphosphate/Calcium Signaling Pathway in Health and Disease. *Physiological Reviews*, *96*(4), 1261–1296. https://doi.org/10.1152/physrev.00006.2016

Bhattacharyya, R., Black, S. E., Lotlikar, M. S., Fenn, R. H., Jorfi, M., Kovacs, D. M., & Tanzi, R. E. (2021). Axonal generation of amyloid-β from palmitoylated APP in mitochondria-associated endoplasmic reticulum membranes. *Cell Reports*, *35*(7). https://doi.org/10.1016/j.celrep.2021.109134

Booth, D. M., Enyedi, B., Geiszt, M., Várnai, P., & Hajnóczky, G. (2016). Redox Nanodomains Are Induced by and Control Calcium Signaling at the

ER-Mitochondrial Interface. *Molecular Cell*, *63*(2), 240–248. https://doi.org/10.1016/j.molcel.2016.05.040
Chang, C.-L., & Liou, J. (2015). Phosphatidylinositol 4,5-Bisphosphate Homeostasis Regulated by Nir2 and Nir3 Proteins at Endoplasmic Reticulum-Plasma Membrane Junctions. *Journal of Biological Chemistry*, *290*(23), 14289–14301. https://doi.org/10.1074/jbc.M114.621375
Cieri, D., Vicario, M., Giacomello, M., Vallese, F., Filadi, R., Wagner, T., Pozzan, T., Pizzo, P., Scorrano, L., Brini, M., & Calì, T. (2018). SPLICS: a split green fluorescent protein-based contact site sensor for narrow and wide heterotypic organelle juxtaposition. *Cell Death & Differentiation*, *25*(6), 1131–1145. https://doi.org/10.1038/s41418-017-0033-z
Clapham, D. E. (2007). Calcium Signaling. *Cell*, *131*(6), 1047–1058. https://doi.org/10.1016/j.cell.2007.11.028
Csordás, G., Renken, C., Várnai, P., Walter, L., Weaver, D., Buttle, K. F., Balla, T., Mannella, C. A., & Hajnóczky, G. (2006). Structural and functional features and significance of the physical linkage between ER and mitochondria. *Journal of Cell Biology*, *174*(7), 915–921. https://doi.org/10.1083/jcb.200604016
de Brito, O. M., & Scorrano, L. (2008). Mitofusin 2 tethers endoplasmic reticulum to mitochondria. *Nature*, *456*(7222), 605–610. https://doi.org/10.1038/nature07534
De Vos, K. J., Mórotz, G. M., Stoica, R., Tudor, E. L., Lau, K.-F., Ackerley, S., Warley, A., Shaw, C. E., & Miller, C. C. J. (2012). VAPB interacts with the mitochondrial protein PTPIP51 to regulate calcium homeostasis. *Human Molecular Genetics*, *21*(6), 1299–1311. https://doi.org/10.1093/hmg/ddr559
Dennis, E. A., & Kennedy, E. P. (1972). Intracellular sites of lipid synthesis and the biogenesis of mitochondria. *Journal of Lipid Research*, *13*(2), 263–267. https://doi.org/10.1016/S0022-2275(20)39421-9
Do, K., & Boxer, S. G. (2011). Thermodynamics, Kinetics, and Photochemistry of β-Strand Association and Dissociation in a Split-GFP System. *Journal of the American Chemical Society*, *133*(45), 18078–18081. https://doi.org/10.1021/ja207985w
Dodig, S., Čepelak, I., & Pavić, I. (2019). Hallmarks of senescence and aging. *Biochemia Medica*, *29*(3), 483–497. https://doi.org/10.11613/BM.2019.030501
Eisenberg-Bord, M., Shai, N., Schuldiner, M., & Bohnert, M. (2016). A Tether Is a Tether Is a Tether: Tethering at Membrane Contact Sites. *Developmental Cell*, *39*(4), 395–409. https://doi.org/10.1016/j.devcel.2016.10.022
Filadi, R., & Pozzan, T. (2015). Generation and functions of second messengers microdomains. *Cell Calcium*, *58*(4), 405–414. https://doi.org/10.1016/j.ceca.2015.03.007

Friedman, J. R., Lackner, L. L., West, M., DiBenedetto, J. R., Nunnari, J., & Voeltz, G. K. (2011). ER Tubules Mark Sites of Mitochondrial Division. *Science*, *334*(6054), 358–362. https://doi.org/10.1126/science.1207385

Fujioka, A., Terai, K., Itoh, R. E., Aoki, K., Nakamura, T., Kuroda, S., Nishida, E., & Matsuda, M. (2006). Dynamics of the Ras/ERK MAPK Cascade as Monitored by Fluorescent Probes. *Journal of Biological Chemistry*, *281*(13), 8917–8926. https://doi.org/10.1074/jbc.M509344200

Gallo, A., Vannier, C., & Galli, T. (2016). Endoplasmic Reticulum–Plasma Membrane Associations: Structures and Functions. *Annual Review of Cell and Developmental Biology*, *32*(1), 279–301. https://doi.org/10.1146/annurev-cellbio-111315-125024

Giacomello, M., & Pellegrini, L. (2016). The coming of age of the mitochondria-ER contact: A matter of thickness. In *Cell Death and Differentiation* (Vol. 23, Issue 9, pp. 1417–1427). Nature Publishing Group. https://doi.org/10.1038/cdd.2016.52

Giordano, F., Saheki, Y., Idevall-Hagren, O., Colombo, S. F., Pirruccello, M., Milosevic, I., Gracheva, E. O., Bagriantsev, S. N., Borgese, N., & De Camilli, P. (2013). PI(4,5)P2-Dependent and Ca2+-Regulated ER-PM Interactions Mediated by the Extended Synaptotagmins. *Cell*, *153*(7), 1494–1509. https://doi.org/10.1016/j.cell.2013.05.026

Haj, F. G., Sabet, O., Kinkhabwala, A., Wimmer-Kleikamp, S., Roukos, V., Han, H.-M., Grabenbauer, M., Bierbaum, M., Antony, C., Neel, B. G., & Bastiaens, P. I. (2012). Regulation of Signaling at Regions of Cell-Cell Contact by Endoplasmic Reticulum-Bound Protein-Tyrosine Phosphatase 1B. *PLoS ONE*, *7*(5), e36633. https://doi.org/10.1371/journal.pone.0036633

Hamasaki, M., Furuta, N., Matsuda, A., Nezu, A., Yamamoto, A., Fujita, N., Oomori, H., Noda, T., Haraguchi, T., Hiraoka, Y., Amano, A., & Yoshimori, T. (2013). Autophagosomes form at ER–mitochondria contact sites. *Nature*, *495*(7441), 389–393. https://doi.org/10.1038/nature11910

Hertlein, K. M., Eddy, B. P., & Lancaster Strickland, M. (2020). A Framework for Assessing Technology-Mediated IPV. *Journal of Couple & Relationship Therapy*, *19*(4), 296–321. https://doi.org/10.1080/15332691.2020.1838377

Heuer, K. H., Mackay, J. P., Podzebenko, P., Bains, N. P. S., Weiss, A. S., King, G. F., & Easterbrook-Smith, S. B. (1996). Development of a Sensitive Peptide-Based Immunoassay: Application to Detection of the Jun and Fos Oncoproteins. *Biochemistry*, *35*(28), 9069–9075. https://doi.org/10.1021/bi952817o

Huang, S.-M., Yang, F., Cai, B.-Y., He, Q.-T., Liu, Q., Qu, C.-X., Han, M.-J., Kong, W., Jia, Y.-L., Li, F., Yu, X., Sun, J.-P., & Wang, J. (2019). Genetically Encoded Fluorescent Amino Acid for Monitoring Protein Interactions through FRET. *Analytical Chemistry*, *91*(23), 14936–14942. https://doi.org/10.1021/acs.analchem.9b03305

Janikiewicz, J., Szymański, J., Malinska, D., Patalas-Krawczyk, P., Michalska, B., Duszyński, J., Giorgi, C., Bonora, M., Dobrzyn, A., & Wieckowski, M. R. (2018). Mitochondria-associated membranes in aging and senescence: Structure, function, and dynamics. *Cell Death and Disease*, *9*(3). https://doi.org/10.1038/s41419-017-0105-5
Kerner, J., & Hoppel, C. (2000). Fatty acid import into mitochondria. *Biochimica et Biophysica Acta (BBA) - Molecular and Cell Biology of Lipids*, *1486*(1), 1–17. https://doi.org/10.1016/S1388-1981(00)00044-5
Kerppola, T. K. (2008). Bimolecular Fluorescence Complementation (BiFC) Analysis as a Probe of Protein Interactions in Living Cells. *Annual Review of Biophysics*, *37*(1), 465–487. https://doi.org/10.1146/annurev.biophys.37.032807.125842
Kumagai, K., & Hanada, K. (2019). Structure, functions and regulation of CERT, a lipid-transfer protein for the delivery of ceramide at the ER–Golgi membrane contact sites. *FEBS Letters*, *593*(17), 2366–2377. https://doi.org/10.1002/1873-3468.13511
Lai, H.-T., & Chiang, C.-M. (2013). Bimolecular Fluorescence Complementation (BiFC) Assay for Direct Visualization of Protein-Protein Interaction in vivo. *BIO-PROTOCOL*, *3*(20). https://doi.org/10.21769/BioProtoc.935
Liu, H. Y., Gale, J. R., Reynolds, I. J., Weiss, J. H., & Aizenman, E. (2021). The Multifaceted Roles of Zinc in Neuronal Mitochondrial Dysfunction. *Biomedicines*, *9*(5), 489. https://doi.org/10.3390/biomedicines9050489
Liu, X., Wen, X., & Klionsky, D. J. (2019). Endoplasmic Reticulum–Mitochondria Contacts Are Required for Pexophagy in *Saccharomyces cerevisiae*. *Contact*, *2*, 251525641882158. https://doi.org/10.1177/2515256418821584
Louche, A., Salcedo, S. P., & Bigot, S. (2017). *Protein–Protein Interactions: Pull-Down Assays* (pp. 247–255). https://doi.org/10.1007/978-1-4939-7033-9_20
Lynes, E. M., Bui, M., Yap, M. C., Benson, M. D., Schneider, B., Ellgaard, L., Berthiaume, L. G., & Simmen, T. (2012). Palmitoylated TMX and calnexin target to the mitochondria-associated membrane. *The EMBO Journal*, *31*(2), 457–470. https://doi.org/10.1038/emboj.2011.384
Missiroli, S., Patergnani, S., Caroccia, N., Pedriali, G., Perrone, M., Previati, M., Wieckowski, M. R., & Giorgi, C. (2018). Mitochondria-associated membranes (MAMs) and inflammation. *Cell Death & Disease*, *9*(3), 329. https://doi.org/10.1038/s41419-017-0027-2
Miyawaki, A., Llopis, J., Heim, R., McCaffery, J. M., Adams, J. A., Ikura, M., & Tsien, R. Y. (1997). Fluorescent indicators for Ca2+based on green fluorescent proteins and calmodulin. *Nature*, *388*(6645), 882–887. https://doi.org/10.1038/42264

Monaco, G., Decrock, E., Akl, H., Ponsaerts, R., Vervliet, T., Luyten, T., De Maeyer, M., Missiaen, L., Distelhorst, C. W., De Smedt, H., Parys, J. B., Leybaert, L., & Bultynck, G. (2012). Selective regulation of IP3-receptor-mediated Ca2+ signaling and apoptosis by the BH4 domain of Bcl-2 versus Bcl-Xl. *Cell Death & Differentiation*, *19*(2), 295–309. https://doi.org/10.1038/cdd.2011.97

Morciano, G., Marchi, S., Morganti, C., Sbano, L., Bittremieux, M., Kerkhofs, M., Corricelli, M., Danese, A., Karkucinska-Wieckowska, A., Wieckowski, M. R., Bultynck, G., Giorgi, C., & Pinton, P. (2018). Role of Mitochondria-Associated ER Membranes in Calcium Regulation in Cancer-Specific Settings. *Neoplasia*, *20*(5), 510–523. https://doi.org/10.1016/j.neo.2018.03.005

Naón, D., Hernández-Alvarez, M. I., Shinjo, S., Wieczor, M., Ivanova, S., Martins de Brito, O., Quintana, A., Hidalgo, J., Palacín, M., Aparicio, P., Castellanos, J., Lores, L., Sebastián, D., Fernández-Veledo, S., Vendrell, J., Joven, J., Orozco, M., Zorzano, A., & Scorrano, L. (2023). Splice variants of mitofusin 2 shape the endoplasmic reticulum and tether it to mitochondria. *Science*, *380*(6651). https://doi.org/10.1126/science.adh9351

Plamont, M.-A., Billon-Denis, E., Maurin, S., Gauron, C., Pimenta, F. M., Specht, C. G., Shi, J., Quérard, J., Pan, B., Rossignol, J., Moncoq, K., Morellet, N., Volovitch, M., Lescop, E., Chen, Y., Triller, A., Vriz, S., Le Saux, T., Jullien, L., & Gautier, A. (2016). Small fluorescence-activating and absorption-shifting tag for tunable protein imaging in vivo. *Proceedings of the National Academy of Sciences*, *113*(3), 497–502. https://doi.org/10.1073/pnas.1513094113

Prinz, W. A., Toulmay, A., & Balla, T. (2020). The functional universe of membrane contact sites. In *Nature Reviews Molecular Cell Biology* (Vol. 21, Issue 1, pp. 7–24). Nature Research. https://doi.org/10.1038/s41580-019-0180-9

Quon, E., Sere, Y. Y., Chauhan, N., Johansen, J., Sullivan, D. P., Dittman, J. S., Rice, W. J., Chan, R. B., Di Paolo, G., Beh, C. T., & Menon, A. K. (2018). Endoplasmic reticulum-plasma membrane contact sites integrate sterol and phospholipid regulation. *PLOS Biology*, *16*(5), e2003864. https://doi.org/10.1371/journal.pbio.2003864

Rainey, K. H., & Patterson, G. H. (2019). Photoswitching FRET to monitor protein–protein interactions. *Proceedings of the National Academy of Sciences*, *116*(3), 864–873. https://doi.org/10.1073/pnas.1805333116

Schauder, C. M., Wu, X., Saheki, Y., Narayanaswamy, P., Torta, F., Wenk, M. R., De Camilli, P., & Reinisch, K. M. (2014). Structure of a lipid-bound extended synaptotagmin indicates a role in lipid transfer. *Nature*, *510*(7506), 552–555. https://doi.org/10.1038/nature13269

Schrader, M., King, S. J., Stroh, T. A., & Schroer, T. A. (2000). Real time imaging reveals a peroxisomal reticulum in living cells. *Journal of Cell Science*, *113*(20), 3663–3671. https://doi.org/10.1242/jcs.113.20.3663
Scorrano, L., De Matteis, M. A., Emr, S., Giordano, F., Hajnóczky, G., Kornmann, B., Lackner, L. L., Levine, T. P., Pellegrini, L., Reinisch, K., Rizzuto, R., Simmen, T., Stenmark, H., Ungermann, C., & Schuldiner, M. (2019). Coming together to define membrane contact sites. *Nature Communications*, *10*(1). https://doi.org/10.1038/s41467-019-09253-3
Shrestha, D., Jenei, A., Nagy, P., Vereb, G., & Szöllősi, J. (2015). Understanding FRET as a Research Tool for Cellular Studies. *International Journal of Molecular Sciences*, *16*(12), 6718–6756. https://doi.org/10.3390/ijms16046718
Simmen, T., Aslan, J. E., Blagoveshchenskaya, A. D., Thomas, L., Wan, L., Xiang, Y., Feliciangeli, S. F., Hung, C.-H., Crump, C. M., & Thomas, G. (2005). PACS-2 controls endoplasmic reticulum–mitochondria communication and Bid-mediated apoptosis. *The EMBO Journal*, *24*(4), 717–729. https://doi.org/10.1038/sj.emboj.7600559
Sohn, M., Korzeniowski, M., Zewe, J. P., Wills, R. C., Hammond, G. R. V., Humpolickova, J., Vrzal, L., Chalupska, D., Veverka, V., Fairn, G. D., Boura, E., & Balla, T. (2018). PI(4,5)P2 controls plasma membrane PI4P and PS levels via ORP5/8 recruitment to ER–PM contact sites. *Journal of Cell Biology*, *217*(5), 1797–1813. https://doi.org/10.1083/jcb.201710095
Stone, S. J., & Vance, J. E. (2000). Phosphatidylserine Synthase-1 and -2 Are Localized to Mitochondria-associated Membranes. *Journal of Biological Chemistry*, *275*(44), 34534–34540. https://doi.org/10.1074/jbc.M002865200
Szabadkai, G., Bianchi, K., Várnai, P., De Stefani, D., Wieckowski, M. R., Cavagna, D., Nagy, A. I., Balla, T., & Rizzuto, R. (2006). Chaperone-mediated coupling of endoplasmic reticulum and mitochondrial Ca2+ channels. *The Journal of Cell Biology*, *175*(6), 901–911. https://doi.org/10.1083/jcb.200608073
Tebo, A. G., & Gautier, A. (2019). A split fluorescent reporter with rapid and reversible complementation. *Nature Communications*, *10*(1). https://doi.org/10.1038/s41467-019-10855-0
van der Veen, J. N., Kennelly, J. P., Wan, S., Vance, J. E., Vance, D. E., & Jacobs, R. L. (2017). The critical role of phosphatidylcholine and phosphatidylethanolamine metabolism in health and disease. *Biochimica et Biophysica Acta (BBA) - Biomembranes*, *1859*(9), 1558–1572. https://doi.org/10.1016/j.bbamem.2017.04.006
Vance, J. E. (1990). Phospholipid synthesis in a membrane fraction associated with mitochondria. *The Journal of Biological Chemistry*, *265*(13), 7248–7256.
Venditti, R., Rega, L. R., Masone, M. C., Santoro, M., Polishchuk, E., Sarnataro, D., Paladino, S., D'Auria, S., Varriale, A., Olkkonen, V. M., Di

Tullio, G., Polishchuk, R., & De Matteis, M. A. (2019). Molecular determinants of ER–Golgi contacts identified through a new FRET–FLIM system. *Journal of Cell Biology*, *218*(3), 1055–1065. https://doi.org/10.1083/jcb.201812020
Verfaillie, T., Rubio, N., Garg, A. D., Bultynck, G., Rizzuto, R., Decuypere, J.-P., Piette, J., Linehan, C., Gupta, S., Samali, A., & Agostinis, P. (2012). PERK is required at the ER-mitochondrial contact sites to convey apoptosis after ROS-based ER stress. *Cell Death & Differentiation*, *19*(11), 1880–1891. https://doi.org/10.1038/cdd.2012.74
von Filseck, J. M., Vanni, S., Mesmin, B., Antonny, B., & Drin, G. (2015). A phosphatidylinositol-4-phosphate powered exchange mechanism to create a lipid gradient between membranes. *Nature Communications*, *6*(1), 6671. https://doi.org/10.1038/ncomms7671
Woehler, A., Wlodarczyk, J., & Neher, E. (2010). Signal/Noise Analysis of FRET-Based Sensors. *Biophysical Journal*, *99*(7), 2344–2354. https://doi.org/10.1016/j.bpj.2010.07.053
Xing, J., Gumerov, V. M., & Zhulin, I. B. (2022). Photoactive Yellow Protein Represents a Distinct, Evolutionarily Novel Family of PAS Domains. *Journal of Bacteriology*, *204*(11). https://doi.org/10.1128/jb.00300-22
Yang, M., Li, C., Yang, S., Xiao, Y., Xiong, X., Chen, W., Zhao, H., Zhang, Q., Han, Y., & Sun, L. (2020). Mitochondria-Associated ER Membranes – The Origin Site of Autophagy. *Frontiers in Cell and Developmental Biology*, *8*. https://doi.org/10.3389/fcell.2020.00595
Young, R. M. (2019). *Proximity Ligation Assay* (pp. 363–370). https://doi.org/10.1007/978-1-4939-9151-8_18
Yu, H., Sun, C., Gong, Q., & Feng, D. (2021). Mitochondria-Associated Endoplasmic Reticulum Membranes in Breast Cancer. *Frontiers in Cell and Developmental Biology*, *9*. https://doi.org/10.3389/fcell.2021.629669
Zal, T., & Gascoigne, N. R. J. (2004). Photobleaching-Corrected FRET Efficiency Imaging of Live Cells. *Biophysical Journal*, *86*(6), 3923–3939. https://doi.org/10.1529/biophysj.103.022087
Zhang, S. L., Yeromin, A. V., Zhang, X. H.-F., Yu, Y., Safrina, O., Penna, A., Roos, J., Stauderman, K. A., & Cahalan, M. D. (2006). Genome-wide RNAi screen of Ca^{2+} influx identifies genes that regulate Ca^{2+} release-activated Ca^{2+} channel activity. *Proceedings of the National Academy of Sciences*, *103*(24), 9357–9362. https://doi.org/10.1073/pnas.0603161103
Ziegler, D. V., Vindrieux, D., Goehrig, D., Jaber, S., Collin, G., Griveau, A., Wiel, C., Bendridi, N., Djebali, S., Farfariello, V., Prevarskaya, N., Payen, L., Marvel, J., Aubert, S., Flaman, J.-M., Rieusset, J., Martin, N., & Bernard, D. (2021). Calcium channel ITPR2 and mitochondria–ER contacts promote cellular senescence and aging. *Nature Communications*, *12*(1), 720. https://doi.org/10.1038/s41467-021-20993-z